AGU PUBLICATIONS

JGR

Journal of Geophysical Research: Solid Earth

RESEARCH ARTICLE
10.1002/2017JB014071

Key Points:
- Faults within the Arbuckle Group reservoir are conductive and penetrate the Precambrian basement
- Mapped faults are critically stressed at depths typical for earthquake hypocenters in southern Kansas and northern Oklahoma
- Reservoir-based slip tendency analysis may be inadequate for assessing reactivation potential of basement faults in the central U.S.

Correspondence to:
T. S. Bidgoli,
tbidgoli@ku.edu

Citation:
Schwab, D. R., Bidgoli, T. S., & Taylor, M. H. (2017). Characterizing the potential for injection-induced fault reactivation through subsurface structural mapping and stress field analysis, Wellington Field, Sumner County, Kansas. *Journal of Geophysical Research: Solid Earth*, *122*, 10,132–10,154. https://doi.org/10.1002/2017JB014071

Received 6 FEB 2017
Accepted 27 OCT 2017
Accepted article online 31 OCT 2017
Published online 13 DEC 2017

Characterizing the Potential for Injection-Induced Fault Reactivation Through Subsurface Structural Mapping and Stress Field Analysis, Wellington Field, Sumner County, Kansas

Drew R. Schwab[1,2], Tandis S. Bidgoli[1,2], and Michael H. Taylor[2]

[1]Kansas Geological Survey, University of Kansas, Lawrence, KS, USA, [2]Department of Geology, University of Kansas, Lawrence, KS, USA

Abstract Kansas, like other parts of the central U.S., has experienced a recent increase in seismicity. Correlation of these events with brine disposal operations suggests pore fluid pressure increases are reactivating preexisting faults, but rigorous evaluation at injection sites is lacking. Here we determine the suitability of CO_2 injection into the Cambrian-Ordovician Arbuckle Group for long-term storage and into a Mississippian reservoir for enhanced oil recovery in Wellington Field, Sumner County, Kansas. To determine the potential for injection-induced earthquakes, we map subsurface faults and estimate in situ stresses, perform slip and dilation tendency analyses to identify well-oriented faults relative to the estimated stress field, and determine the pressure changes required to induce slip at reservoir and basement depths. Three-dimensional seismic reflection data reveal 12 near-vertical faults, mostly striking NNE, consistent with nodal planes from moment tensor solutions from recent earthquakes in the region. Most of the faults cut both reservoirs and several clearly penetrate the Precambrian basement. Drilling-induced fractures ($N = 40$) identified from image logs and inversion of earthquake moment tensor solutions ($N = 65$) indicate that the maximum horizontal stress is approximately EW. Slip tendency analysis indicates that faults striking <020° are stable under current reservoir conditions, whereas faults striking 020°–049° may be prone to reactivation with increasing pore fluid pressure. Although the proposed injection volume (40,000 t) is unlikely to reactive faults at reservoir depths, high-rate injection operations could reach pressures beyond the critical threshold for slip within the basement, as demonstrated by the large number of injection-induced earthquakes west of the study area.

1. Introduction

Injection-induced earthquakes are a growing concern near underground injection control (UIC) class II wells across the central and eastern U.S. (CEUS). These wells dispose of fluid waste, coproduced with oil and gas, injecting it into subsurface reservoirs for long-term storage and for secondary oil and gas recovery. Since 2009, the number and rate of earthquakes near such injection operations have sharply increased, including areas in Kansas (e.g., Buchanan, 2015), Texas (e.g., Frohlich, 2012), Arkansas (e.g., Horton, 2012), Ohio (e.g., Kim, 2013), New Mexico (e.g., Rubinstein et al., 2014), and Oklahoma (e.g., Keranen et al., 2014). Although the vast majority of class II wells across the country operate without incident (e.g., Ellsworth, 2013; Weingarten et al., 2015), the recent surge in seismicity has challenged assumptions about the safety and efficacy of underground fluid injection (brine or CO_2) (e.g., Zoback & Gorelick, 2012). At the same time, booming development of unconventional (i.e., low permeability) resource plays that typically have high water-to-oil ratios and increased regulation on the emissions of greenhouse gases (CO_2) mean that the need for additional injection wells is growing, as are the operational demands on existing wells.

One of the principal causes of induced seismicity is injection of wastewater into deep strata or basement formations near preexisting faults (e.g., Ellsworth, 2013; Evans, 1966; Healy et al., 1968; Raleigh et al., 1976; Zoback & Gorelick, 2012). Typically, faults will not reactivate as long as the applied shear stress is less than the stress of the contact. The failure condition is expressed by the equation $\tau_{crit} = \mu(\sigma_n - P) + \tau_o$, where τ_{crit} is the critical shear stress, μ is the coefficient of friction (0.6 to 1.0), σ_n is the effective normal stress, P is the pore pressure, and τ_o is the cohesive strength. This equation is then modified for Byerlee material (cohesionless fault) in which there is no shear strength ($\tau_o = 0$) (Byerlee, 1978). Failure can occur by increasing the shear stress, reducing the normal stress, and/or elevating the pore fluid pressure. The likelihood of an induced

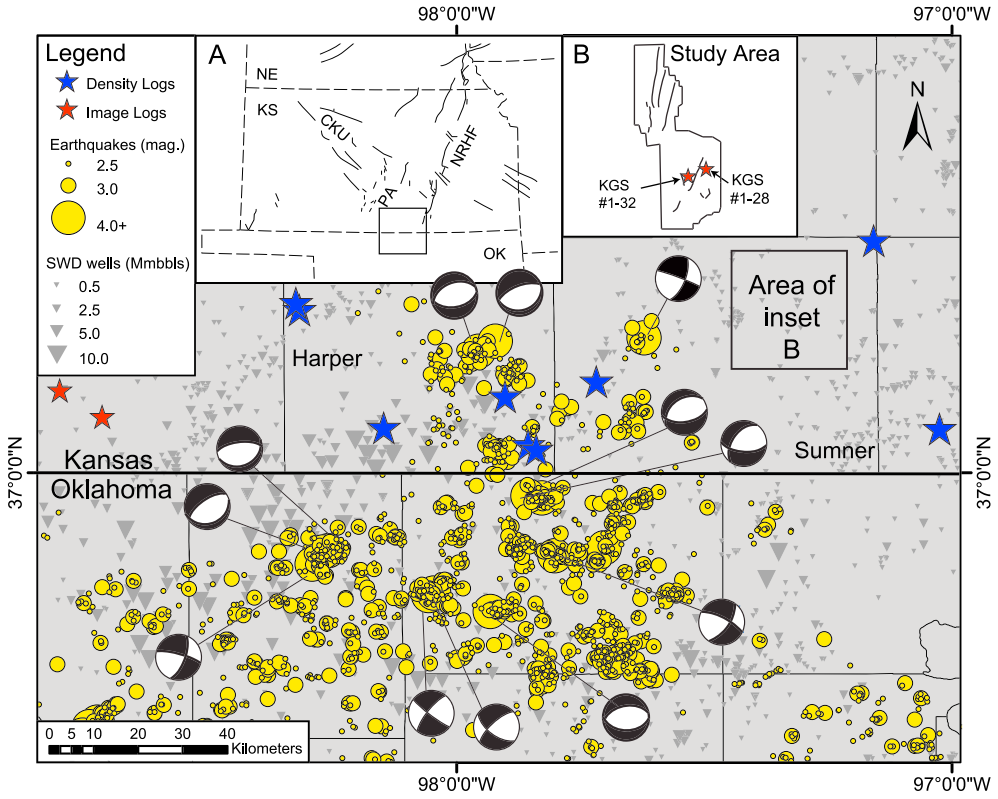

Figure 1. Earthquake data ($M > 2.5+$, 1 (yellow circles) gray circles; $N = 3903$), including earthquake moment tensor solutions focal mechanisms ($N = 70$) for $M3.0$ (small circle) and $M4.0+$ (large circle) earthquakes, were collected from the NEIC ANSS from 1/12 to −4/16 for south central Kansas and north central Oklahoma. Earthquakes are in close proximity to high- rate injection wells (grey triangles). Stress orientations and magnitudes were estimated using image (red stars) and density log (blue stars) data (orange stars) from wells in Barber, Harper, Sumner, and Cowley counties, including the KGS 1–28 and KGS 1–32 wells, which had both density and image logs. Inset A shows major structural elements in Kansas, from Hildebrand et al. (1988). CKU: Central Kansas Uplift, NRHF: Nemaha Ridge-Humboldt fault zone, and PA: Pratt Anticline. Inset B shows areal extent of 3-D seismic data across Wellington Field in the south and Anson Bates Field in the north, with 12 projected fault planes.

event is dependent on (1) the magnitude of the pore fluid pressure perturbation, (2) the spatial extent of the pore fluid pressure change, (3) ambient stress conditions close to failure conditions, and (4) faults that are optimally oriented for failure (Ellsworth, 2013). The rate of injection (e.g., Weingarten et al., 2015) and the presence of a hydraulic connection to deeper faults (e.g., Townend & Zoback, 2000) can also influence the likelihood for induced events.

The challenges associated with class II injection are well typified by the subsurface geology and oil and gas fields of south central Kansas. Historical seismicity in this region, like other parts of the midcontinent, has been low. Low strain rates (Argus & Gordon, 1996; Calais et al., 2006) combined with thick (305 m), permeable (up to 1,500 mdarcy), deep (1,270 m), and well-confined reservoir conditions have made the Cambrian-Ordovician Arbuckle Group a prime brine disposal reservoir for decades (Franseen et al., 2004). However, concentrated and high-rate brine disposal into the Arbuckle since 2012 has led to increased seismicity in this part of Kansas, with more than 100 $M3.0+$ earthquakes since 2013, including a $M4.9$ in western Sumner County and $M4.3$ and $M4.1$ in central Harper County (Figures 1 and 2) (from the National Earthquake Information Center(NEIC) Advanced National Seismic System (ANSS) Composite Catalog). The majority of these events have occurred within the crystalline basement, at depths of 3–7 km, well below the primary injection interval, suggesting a hydraulic connection with basement faults. A major challenge for stakeholders in Kansas and other parts of the CEUS is that subsurface faults and stresses are not well known, making it difficult to properly site new disposal wells or make informed decisions regarding existing disposal wells. Industry 2-D and 3-D seismic reflection data sets that could aid in identifying subsurface faults are generally lacking, and well log data that can provide constraints on the in situ stresses have not been rigorously evaluated. Such detailed characterization of subsurface faults and in situ stresses is critical for accurate assessments of the potential for induced seismic hazards.

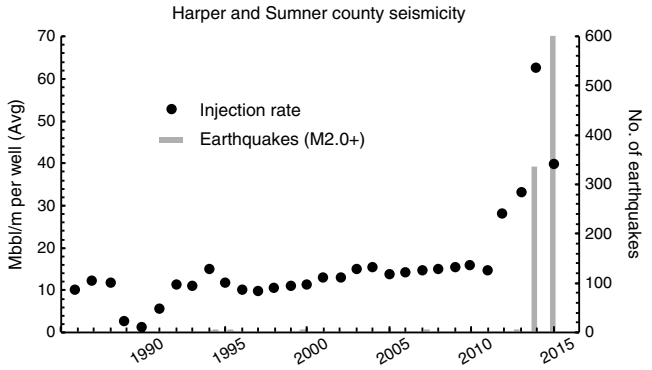

Figure 2. Saltwater disposal (Class II) injection rates and earthquakes in Harper and Sumner counties from 1985 to 2015. The average injection rate per disposal well increased significantly in 2012. Seismicity near the injection wells in Harper and Sumner counties has increased significantly since 2013 (bars; *M*2.0+). Earthquake data from the NEIC ANSS catalog. Saltwater disposal volumes provided by the Kansas Corporation Commission.

This study focuses on evaluating the potential for induced seismicity associated with fluid injection into two reservoirs in Wellington Field, north central Sumner County. The field is the site of a small-scale CO_2 injection project (Figure 1) and is good analog for understanding the relationships between subsurface geology, fluid injection, and seismicity within the midcontinent. Target injection depths are within the Mississippian Series (1,116–1,129 m) for the purpose of enhanced oil recovery (EOR) and the Cambrian-Ordovician Arbuckle Group (1,496–1,539 m) for the purpose of long-term storage. Both the Mississippian Series and the Arbuckle Group are deep, heterogeneous limestone-dolomite reservoirs (Goebel, 1966; Walters, 1958; Zeller, 1968). The combination of 3-D seismic reflection data, image logs, and test data (e.g., pump tests) enables a more robust analysis of potential faults and reservoir conditions, not typically available at injection sites across the U.S. midcontinent. Such analyses can provide a better understanding of injection conditions that lead to induced earthquakes, including whether the proposed volume of CO_2 (40,000 t) poses any seismic hazard.

This paper focuses on determining the likelihood of slip for faults within Wellington Field. The suitability of injection in the field is evaluated for both the proposed CO_2 injection volume (40,000 t) and for commercial-scale fluid injection of brine or CO_2. Through 3-D seismic mapping of faults and detailed stress field analysis, we show that under current reservoir conditions, faults appear to be stable and require pore fluid pressure changes of 1.1–9.7 MPa, much higher than the estimated pressure change (0.4 to $<$0.15 MPa) for the proposed injection volumes. However, the occurrence of nearby induced events below the injection reservoirs, within the Precambrian basement, suggests the presence of large, conductive, and critically stressed faults that may reactivate in response to small pore fluid pressure change. Therefore, although our results suggest a low likelihood for injection-induced fault reactivation associated with pilot-scale injection, we show that reservoir-based assessments may be inadequate for proper hazard characterization for faults within the Precambrian crystalline basement.

2. Study Area

Wellington Field encompasses approximately a 20.7 km^2 area of north central Harper County (Figure 1). The oil field was discovered in 1929 and has produced more than 20 million barrels of oil over its history, through nearly 300 wells and successful waterflood operations (KGS oil and gas wells database, 2016). Current oil production has slowed to 55 producing wells (KGS oil and gas wells database, 2016). Production in the field and recent CO_2-EOR efforts are focused on Mississippian reservoirs, while the underlying Arbuckle Group saline aquifer system is routinely used in the region for wastewater (UIC class II) and hazardous waste (UIC class I) disposal and is the proposed target for long-term storage of CO_2.

Wellington Field resides in the southern part of the Sedgwick Basin, which is bounded by the Nemaha Ridge-Humboldt fault zone (NRHF) to the east and Pratt anticline and Central Kansas Uplift (CKU) to the west. The ~50 km wide, NNE trending NRHF extends 500 km from Nebraska to Oklahoma and borders the Forest City Basin to the east and the Salina Basin to the west (Lee & Merriam, 1954; Lugn, 1935; Stander & Grant, 1989; Steeples et al., 1979). The NRHF is one of several regional structures within the U.S. midcontinent that has been identified from subsurface data, including potential field anomalies (e.g., Kruger, 1997), limited seismic reflection data (e.g., Steeples et al., 1979; Stander & Grant, 1989), and well log data (e.g., McBee, 2003). A number of faults are associated with the NRHF system, including the Humboldt fault, a strike-slip fault located on the eastern flank of the NRHF. The NRHF has also been seismically active, with a number of historical and recent earthquakes occurring along its extent (DuBois & Wilson, 1978; Gerhard, 2004; Hildebrand et al., 1988; Merriam, 1956; Steeples & Brosius, 1996).

The NRHF system strikes subparallel to the late Precambrian Midcontinent Rift System (MRS), which is approximately 40 km to the west. The NRHF and MRS appear to have similar tectonic origin, as

evidenced by the geometry of the NRHF and by lower Paleozoic erosion and sedimentation that appears to be affected by NRHF movement (Gerhard, 2004). The MRS occurs from central Kansas to the northeast through Nebraska, Iowa, and Minnesota, terminating near the Lake Superior region. Rifting stopped after spreading only 50–80 km (Steeples & Brosius, 1996; Woelk & Hinze, 1995). The MRS is recognized by a positive central high and flanking minima on both gravity and magnetic maps, which suggests a horst and graben geometry (Hinze, 1963; Hinze et al., 1982; King & Zietz, 1971; Lyons, 1959; Oray et al., 1973; Thiel, 1956).

To the west of the study area is the Central Kansas Uplift, a regional NW trending structural feature that occupies much of the central part of the state (Koester, 1935; Merriam, 1963). It is an important feature for petroleum exploration and production and was originally revealed by drilling operations. The structure developed through several periods of warping and faulting as early as Precambrian time, with folding occurring primarily in the Pennsylvanian and post-Cretaceous interval (Koester, 1935). Along the flanks and crests of the CKU are secondary structures, including prominent anticlines and strike-slip and normal faults that are generally stable but have experienced recent seismicity (Merriam, 1963). Also, to the west of the study area is the Pratt anticline, a broad, south plunging fold that initiated due to deformation in the Early Paleozoic and reactivated in pre-Desmoinesian post-Mississippian time (Merriam, 1963).

The NRHF, MRS, and CKU are continental-scale features that are associated with myriad of smaller-scale faults developed within the shallower Paleozoic stratigraphy. Baars and Watney (1991) show that for many of the major stratigraphic packages in Kansas (e.g., Arbuckle Group, Mississippian, and Lansing-Kansas City groups), erosion, facies patterns, and diagenesis are all strongly influenced by tectonics, suggesting that reactivation of basement faults occurred many times prior to well-documented Pennsylvanian exhumation and erosion of the NRHF and CKU. Episodic reactivation of basement structures is also consistent with the distribution of historic and instrumentally recorded earthquakes across the state, which are generally aligned with these known structures.

2.1. Injection Reservoirs

The Mississippian Series is made up of interlayers of limestone and chert that can be divided into two lithological sequences. In Wellington Field, the Upper Mississippian Series consist of ~70 m of argillaceous limestone and lime mudstone interbedded with chert, bounded at the top by an unconformity (Scheffer, 2012). This interval is the oil-producing zone in the field and is the proposed target for CO_2 injection for EOR. The Lower Mississippian Series (~50 m) consists mainly of argillaceous limestones and argillaceous dolomitic siltstones that may serve as suitable seals for the Arbuckle aquifer (Scheffer, 2012).

The Cambro-Ordovician Arbuckle Group is the proposed reservoir for carbon capture and storage (CCS) (Figure 3). The Arbuckle Group consists primarily of dolomitic limestone interbedded with shale and has been divided into three formations: the Jefferson City-Cotter Dolomite, Roubidoux Formation, and Gasconade Dolomite-Gunter Sandstone (Cole, 1975; Franseen, 2000; Merriam, 1963). The proposed injection interval for CO_2-CCS lies at the base of the Gasconade Dolomite (1,496–1,539 m), a 77 m thick, coarsely granular dolomite that rests unconformably on the Precambrian basement (Figure 3).

The Upper Devonian to Lower Mississippian Chattanooga Shale is the primary seal for CCS in the Arbuckle Group (Figure 3). The Chattanooga Shale is dolomitic and silty and ranges in thickness regionally from 1 to 50 m (Goebel, 1968; Lee, 1940; Zeller, 1968). Well logs at KGS 1–28 indicate a thickness of 15 m; however, core at KGS 1–32 indicated a thickness of only 15 cm (Scheffer, 2012).

Across much of Kansas, Arbuckle Group and Mississippian Series reservoir pressures are below hydrostatic (Bradley, 1975; Nelson & Gianoutsos, 2011; Puckette & Al-Shaieb, 2003; Sorenson, 2005). The abnormally low reservoir pressure is a consequence of the departure between surface elevations and hydraulic head, which is the result of a major hydrodynamic adjustment associated with post-Laramide uplift, erosion, and formation water discharge (Nelson & Gianoutsos, 2011; Sorenson, 2005). Oil and gas production from the Mississippian has resulted in further reduction of ambient fluid pressures, down to 6.2 MPa (~5 MPa below hydrostatic) in the field. These subnormal reservoir pressures attest to the adequacy and regional extent of seals and make these vertically confined reservoirs ideal for fluid injection.

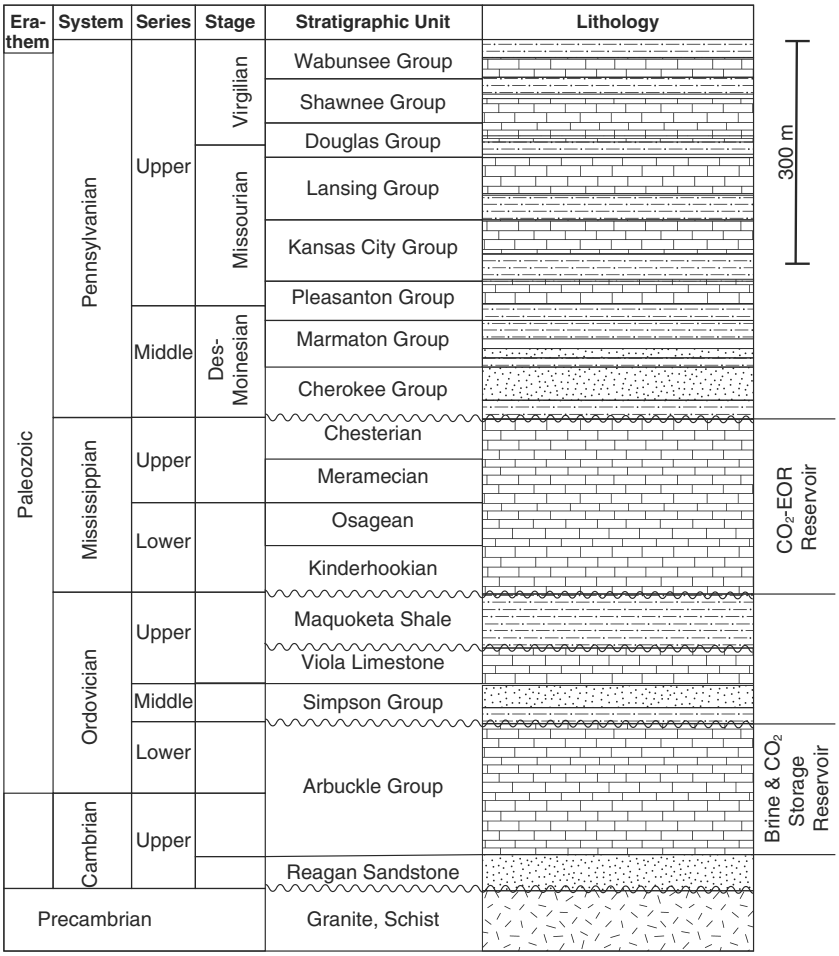

Figure 3. Stratigraphic column showing major stratigraphic units across Kansas. Modified from Carr et al. (2005).

3. Methods

3.1. Fault Mapping and Characterization

To determine fault geometries, we used 3-D seismic reflection data across the study area, which includes Wellington Field to the south and Anson Bates Field to the north. The 3-D seismic data volume covers a 41.3 km^2 area across these fields, to a depth of 1.89 km, and contains 541 in-lines and 251 cross-lines. Acquisition and processing of the seismic reflection data were optimized for imaging the Arbuckle Group and Mississippian Series; therefore, data quality and resolution are diminished, in some instances, below the Arbuckle.

Faults and stratigraphic horizons were mapped using standard seismic interpretation procedures in Schlumberger's Petrel™, a Windows-based commercial software for subsurface geophysical interpretation and geologic modeling. Stratigraphic horizons were tied to the seismic reflection data using 210 wells, and top reflectors for the basement, Arbuckle Group, Mississippian Series, Kansas City Limestone, and Topeka Limestone were mapped. Faults were mapped in vertical seismic reflection profiles by identifying offsets or discontinuities in these and other arbitrary horizons. Depth slices were also useful in identifying faults and determining the lateral extent of faults by locating abrupt breaks in reflection amplitude (Bahorich & Farmer, 1995). To increase confidence in our fault interpretations, we used seismic attributes like coherency to highlight trace-to-trace variability and changes in acoustic impedance that may be associated with faults (Bahorich & Farmer, 1995). We then evaluated the mapped faults using several criteria, including (1) fault geometry, (2) fault length-to-width and length-to-displacement ratios (e.g., Hanks & Bakun, 2008; Wells & Coppersmith, 1994), (3) continuity between seismic profiles, and (4) consistency with other known geological structures (e.g., Lee & Merriam, 1954; Lugn, 1935; Stander & Grant, 1989; Steeples et al., 1979). Fault geometry

Table 1
Fault Characteristics

Fault #	Strike (deg)	Dip (deg)	Length (m)	Width (m)	Vertical separation (m)
1	6	90	4450+	883+	22
2	13	90	2173	914+	30
3	12	90	4267+	990+	33
4	165	70°SE	290	99	21
5	11	71.5°E	1441	98	29
6	10	88°W	210	206	25
7	26	75°SE	2652	411	22
8	166	86°SW	930	274	12
9	170	75°E	303	274	22
10	17	83°SE	503	274	18
11	145	80°SW	396	414	12
12	13	51°SE	945	62	22

was measured in Petrel for strike, dip, length, width, and vertical separation (Table 1). Faults and stratigraphic horizons were then modeled as 3-D surfaces to visualize spatial relationships and to identify any inconsistent interpretations.

3.2. Stress Orientations

Assuming one of the principle stresses is the vertical stress (S_v), the orientation of the maximum and minimum horizontal stresses (SH_{max} and Sh_{min}, respectively) can be determined by analyzing image and other types of well logs for drilling-induced tensile fractures (Aadnoy, 1990; Moos & Zoback, 1990; Wiprut & Zoback, 2000) and borehole breakouts (Bell & Gough, 1979; Zoback et al., 2003, 1985). In an open hole, circumferential stresses concentrate around the wellbore walls and are variable with azimuth. The circumferential stress is lowest at the azimuth of the SH_{max} and highest at the azimuth of the Sh_{min}. Drilling-induced tensile fractures initiate parallel to the direction of SH_{max} when the wellbore wall goes into tension, which is often the case when there are large differences between Sh_{min} and SH_{max} (Aadnoy, 1990; Moos & Zoback, 1990). Drilling-induced tensile fractures appear on image logs as narrow, well-defined conductive features separated by 180° (Tingay et al., 2008). In contrast, borehole breakouts occur parallel to Sh_{min}, when the circumferential stress exceeds the compressive strength of the rock at the wellbore (Bell, 1990; Tingay et al., 2008; Zoback et al., 1985). Borehole breakouts appear on image logs as broad, parallel, often poorly resolved conductive features separated by 180° (Tingay et al., 2008).

We analyzed image logs from two wells within Wellington Field for borehole stress indicators: the KGS 1–28 and KGS 1–32 wells (Figure 1). To evaluate potential variability in the stress field across the region, image logs from an additional four wells in nearby counties were also analyzed (Figure 1). Of the six wells evaluated, four had drilling-induced tensile fractures. No borehole breakouts were identified. Individual fractures varied in orientation from top to bottom, with up to 010° of deviation. Measurements were taken near the top and the base of each individual fracture. Exact measurement locations varied and were dependent on the best representation as determined by the interpreter. All of the measurements were then averaged to estimate the orientation of SH_{max}. A quality ranking system, established by Zoback and Zoback (1991), was used to characterize the accuracy of measurements taken from each well (Table 2). Generally, estimates are considered of higher quality (A rating) when there were larger numbers of distinct measurements, larger sizes of the fractures or breakouts, and smaller deviations between distinct measurements.

Earthquake moment tensor solutions are also a widely used present-day stress indicator (e.g., Gephart & Forsyth, 1984; McKenzie, 1969; Michael, 1984, 1987; Yih-Hsiung et al., 1991; Zoback et al., 1989). Although the azimuth and plunge of the principal axes of moment tensor solutions are not directly equivalent to the principal stress axes, one can use them as an indirect approximation of the stress field (e.g., McKenzie, 1969). Several computer-based inversion programs have been developed with consistent results, suggesting that inversion of moment tensor solutions is a reasonable estimator for stress orientations (Angelier, 1979; Ellsworth, 1982; Ellsworth & Zhonghuai, 1980; Gephart & Forsyth, 1984; Michael, 1984). The software package used in this study, STRESSInverse, was modeled after the method demonstrated by Michael (1984, 1987) (Vavryčuk, 2014). By this method, using the tangential traction on a number of planes in a region and by assuming that the slip events are independent and represent the same stress tensor, it is possible to determine the stress field. The result is a single uniform stress tensor that most likely influenced the faulting events (Michael, 1984, 1987; Vavryčuk, 2014).

For this study, we inverted 66 moment tensor solutions from recent injection-induced earthquakes in south central Kansas and north central Oklahoma for principal stress directions (Figure 1 and Table 3). Earthquake moment tensor solutions were obtained from the NEIC ANSS Composite Catalog for earthquakes of moment magnitude 3.0 and greater from 1 January 2012, through 28 April 2016. Input parameters for the inversion are strike, dip, and rake associated with one of the nodal planes. The nodal plane selected for inversion was the plane consistent with both the fault plane orientations observed in the study area and the known structures in the region, primarily with nodal planes striking approximately NNE. Although it is not necessary to use the

Table 2
Drilling-Induced Tensile Fractures

McGrath 1–16 (C)			Spriggs 1–34 (B)			KGS 1–28 (C)			KGS 1–32 (C)		
Azimuth #1 (deg)	Azimuth #2 (deg)	Height (m)	Azimuth #1 (deg)	Azimuth #2 (deg)	Height (m)	Azimuth #1 (deg)	Azimuth #2 (deg)	Height (m)	Azimuth #1 (deg)	Azimuth #2 (deg)	Height (m)
81	86	3	79	84	2	79	80	30	66	71	40
81	81	5	79	61	3	81	81	2	78	66	35
76	81	4	81	84	2	63	80	12	55	76	15
81	81	2	79	59	1	73	79	11	71	77	43
83	81	6	78	76	3	77	79	3	66	81	200
81	81	4	71	74	3						
81	81	1	79	80	5						
81	81	2	77	79	2						
84	81	2	83	81	7						
83	79	4	71	72	29						
82	82	1	79	81	21						
81	87	4	76	81	5						
81	80	5	61	71	7						
84	84	26	83	87	14						
81	81	6	63	71	21						

nodal plane that represents the actual fault plane, doing so will result in better confidence regions and better allows the algorithm to manipulate the data set to find an acceptable uniform stress field (Michael, 1987). Both strike-slip (SS) and normal-slip (NS) moment tensor solutions were available. Because the orientation of σ_1 is different for SS and NS stress environments, the inversion was done separately for SS and NS moment tensors solutions to avoid conflicting inputs and to prevent inaccurate results. We note that SS and NS moment tensors solutions occur in close proximity to one another, suggesting that the stress magnitude of both principal axes is similar as well. Stress inversion of the moment tensor solutions had up to 2,000 iterations using a bootstrap resampling method to ensure a higher confidence in the result. Bootstrap resampling randomly selects moment tensor data for the given sample size, in our case $N = 36$ (SS) and $N = 30$ (NS), with some moment tensors repeated, while others are absent. Repeating this process over many iterations reveals the true variation in the data, with a result that more closely resembles the best fit stress field (Michael, 1987).

3.3. Stress Magnitudes

The vertical stress (S_v) was estimated using density logs in 11 wells in south central Kansas, including KGS 1–28 and KGS 1–32 (Figure 1). The overburden stress is calculated by a depth integration of density using the following equation:

$$S_v = \int_0^z \rho(z) g dz \approx \overline{\rho} g z$$

where $\rho(z)$ is the density as a function of depth, g is the gravitational acceleration, and $\overline{\rho}$ is mean overburden density (Zoback et al., 2003). The calculation assumes that hydrostatic pore pressure increases at a rate of 9.8 MPa/km (Zoback et al., 2003).

To ensure accuracy, only wells for which density logs reached the base of the Arbuckle or deeper were used. Overburden estimates at depths beyond the measured data were calculated by using a uniform density of 2.75 g/cm^3. This value was derived from accepted basement rock density averages and is in agreement with shallow basement density measurements taken from density logs in south central Kansas (Smithson, 1971).

To estimate the magnitude of Sh_{min}, step rate test data from KGS 1–32 was analyzed at a gauge depth of 1,484 m. Both the breakdown pressure (the pressure required to initiate a fracture) and the closure pressure (the pressure required to hold a fracture open) were identified (FazelAlavi, 2015). Because the pressure needed to close a fracture is controlled by the magnitude of the least principal stress, the closure pressure is the best approximation of the magnitude of Sh_{min} (Nelson et al., 2007; Zoback et al., 2003).

Table 3
Moment Tensor Nodal Planes for Inversion

Date and time	Magnitude	Location	Strike (deg)	Dip (deg)	Rake (deg)
		Strike slip			
2016-02-06T20:39:09.000Z	3.4	36.827°N, 97.775°W	48	85	160
2016-01-26T06:24:49.700Z	3.2	36.918°N, 97.982°W	36	80	−175
2015-11-30T09:49:12.800Z	4.7	36.751°N, 98.056°W	219	75	−173
2015-11-24T00:54:18.200Z	3.3	36.818°N, 98.285°W	224	60	−145
2015-11-09T22:42:06.600Z	3.6	37.122°N, 97.617°W	206	74	167
2015-10-30T04:37:02.220Z	3.4	37.152°N, 97.623°W	0	90	160
2015-10-19T04:55:29.400Z	3.1	36.735°N, 97.840°W	50	90	−175
2015-08-22T08:46:49.500Z	3.8	36.842°N, 97.827°W	217	73	−162
2015-08-14T21:25:40.600Z	4.1	36.831°N, 97.801°W	35	64	−162
2015-06-27T03:31:28.200Z	3.5	36.746°N, 98.224°W	244	80	−179
2015-05-23T10:46:42.300Z	3.2	36.849°N, 97.698°W	238	86	−171
2015-04-20T12:08:31.400Z	3.4	36.849°N, 97.880°W	61	85	−165
2015-04-18T18:34:04.800Z	3.4	36.945°N, 97.631°W	51	64	180
2015-03-24T15:31:51.490Z	3.7	37.105°N, 97.650°W	6	86	−179
2015-02-15T18:27:08.430Z	3.6	37.187°N, 97.900°W	180	80	−5
2015-02-05T15:08:40.800Z	4.2	36.815°N, 98.291°W	20	67	−167
2015-02-04T13:20:31.880Z	3.4	37.189°N, 97.901°W	44	60	−145
2015-02-01T18:06:04.000Z	3.7	36.945°N, 97.630°W	60	85	20
2015-01-30T14:24:22.100Z	3.6	36.808°N, 98.364°W	230	81	172
2015-01-29T20:21:38.710Z	3.4	37.185°N, 97.856°W	30	80	180
2015-01-25T09:36:32.200Z	3.7	36.952°N, 97.615°W	24	75	168
2015-01-24T15:36:46.500Z	3.4	36.807°N, 98.360°W	44	76	154
2015-01-19T10:19:20.200Z	3.8	36.803°N, 98.196°W	198	75	−153
2015-01-19T09:54:31.660Z	3.5	37.215°N, 97.872°W	212	51	−164
2014-12-11T07:53:49.400Z	3.8	36.762°N, 98.054°W	35	78	154
2014-11-25T14:43:40.000Z	3.6	36.820°N, 97.719°W	24	72	−173
2014-09-08T12:56:52.900Z	3.4	37.263°N, 97.635°W	355	65	−30
2014-08-17T15:59:05.600Z	3.1	36.858°N, 97.871°W	30	84	−156
2014-08-17T06:31:10.300Z	3.2	36.852°N, 97.869°W	203	80	−166
2014-08-17T06:18:43.200Z	3.4	36.861°N, 97.873°W	24	86	166
2014-08-01T14:44:27.700Z	3.2	36.762°N, 98.044°W	218	75	−170
2014-08-01T14:19:21.100Z	3.1	36.750°N, 98.045°W	46	64	−146
2014-07-29T02:46:36.000Z	4.3	36.756°N, 98.045°W	227	71	−149
2014-06-26T14:02:50.200Z	3.2	36.868°N, 97.688°W	45	90	180
2014-06-23T13:44:59.400Z	3.4	36.851°N, 97.856°W	205	90	175
2014-03-16T08:46:20.180Z	3.7	37.192°N, 97.899°W	193	72	−154
		Normal slip			
2016-01-14T23:15:31.900Z	3.5	36.939°N, 97.797°W	85	60	−65
2015-12-04T05:08:12.900Z	3.2	36.831°N, 98.274°W	80	65	−60
2015-11-30T21:28:44.400Z	3.3	36.944°N, 97.831°W	265	70	−75
2015-11-26T00:56:02.500Z	3.1	36.946°N, 97.811°W	260	75	−60
2015-11-23T21:17:46.500Z	4.4	36.838°N, 98.276°W	72	26	−75
2015-11-20T22:55:51.200Z	3.5	36.941°N, 97.826°W	82	62	−76
2015-11-20T22:40:40.300Z	4.1	36.948°N, 97.828°W	85	54	−73
2015-11-11T01:39:03.600Z	3.5	36.947°N, 97.826°W	100	65	−55
2015-11-07T18:29:13.400Z	3.8	36.947°N, 97.837°W	105	58	−47
2015-11-07T11:11:53.900Z	4.1	36.953°N, 97.855°W	94	60	−51
2015-10-17T13:20:00.640Z	3.4	37.057°N, 97.934°W	59	62	−112
2015-10-17T12:12:49.970Z	3.4	37.054°N, 97.941°W	61	52	−102
2015-08-20T00:47:12.700Z	3.6	36.844°N, 98.269°W	43	45	−123
2015-07-21T11:16:13.800Z	3.1	36.837°N, 98.245°W	53	40	−116
2015-07-20T20:54:32.100Z	3.7	36.846°N, 98.252°W	38	46	−129
2015-07-20T20:19:03.400Z	4.4	36.842°N, 98.259°W	65	26	−107
2015-06-05T23:12:47.450Z	4.1	37.265°N, 97.921°W	76	25	−83
2015-05-30T11:21:40.050Z	3.6	37.041°N, 97.905°W	63	51	−124
2015-02-13T17:42:40.900Z	3.4	36.952°N, 97.624°W	288	50	−94
2014-12-14T09:14:21.100Z	3.9	36.871°N, 98.127°W	82	24	−86
2014-11-24T19:05:57.500Z	3.7	36.873°N, 98.335°W	84	37	−62
2014-11-15T10:18:13.470Z	3.8	37.229°N, 98.033°W	103	37	−54

Table 3 *(continued)*

Date and time	Magnitude	Location	Strike (deg)	Dip (deg)	Rake (deg)
		Normal slip			
2014-10-02T18:01:24.400Z	4.3	37.245°N, 97.955°W	81	48	−81
2014-09-30T14:55:04.650Z	3.8	37.221°N, 97.963°W	87	34	−67
2014-09-08T16:21:34.000Z	3.9	36.821°N, 97.722°W	34	37	−108
2014-08-18T01:25:57.400Z	3.7	36.840°N, 98.254°W	86	33	−76
2014-04-07T03:25:34.000Z	3.4	36.841°N, 98.278°W	93	33	−63
2014-02-03T09:03:21.580Z	3.6	37.132°N, 97.768°W	57	48	−59
2013-12-29T02:41:02.400Z	3.6	36.958°N, 97.670°W	105	62	−113
2013-12-16T15:09:53.900Z	3.8	37.130°N, 97.776°W	251	64	−62

For comparison, another pump test in Harper County (Yeti 1–15 well in the Wharton South Field) was analyzed and the breakdown pressure was identified, but no closure pressure was interpreted from the data.

Calculation of SH_{max} was completed through use of equations (1) and (2), which are considered an acceptable method for estimating SH_{max} when drilling-induced tensile fractures are present in a borehole (Zoback et al., 2003). Equation (1) was derived from equation (3), which represents the conditions at which a tensile fracture in the wall of a vertical wellbore occurs (Zoback et al., 2003). Zoback et al. (2003) shows that it is acceptable to assume that ΔP and $\sigma^{\Delta T}$ are close to 0 by comparing results of equation (1) with estimated stress polygon values. Equation (2) was used to account for any uncertainty in the pore fluid pressure (Pp) at depth:

$$SH_{max} = 3SH_{min} - 2Pp \tag{1}$$

$$SH_{max} = 3SH_{min} - Pp \tag{2}$$

$$3SH_{min} - SH_{max} - 2\,Pp - \Delta P - \sigma^{\Delta T} = 0 \tag{3}$$

Stress magnitudes at basement depth (5.85 km) were calculated using a stress polygon (e.g., Zoback et al., 2003) for a coefficient of friction (μ) of 0.6 (Byerlee, 1978). Boundaries of the stress polygon represent the failure limits for different stress states (NS, SS, or RS). Boundaries were defined by the following equations (Moos & Zoback, 1990; Zoback et al., 1987):

$$F(\mu) = \left[\mathrm{sqrt}\left(\mu^2 + 1\right) + \mu\right]^2 \tag{4}$$

$$SH_{max} = F(\mu)(S_v - Pp) + Pp \tag{5}$$

$$SH_{min} = (S_v - Pp)/f(\mu) + Pp \tag{6}$$

Pore fluid pressures were determined from shut-in or stabilization pressures obtained during step-rate and drill stem tests (DSTs) in the KGS 1–28 and KGS 1–32 wells (FazelAlavi, 2015). Shut-in pressures were measured at a gauge depth of 1,523 m (KGS 1–28) and 1,484 m (KGS 1–32) in the Arbuckle during step rate tests (FazelAlavi, 2015). DST-based reservoir pressure determinations (P^*) were calculated for tested intervals of the Mississippian and Arbuckle in both wells using Horner plots developed from initial and final shut-in pressures and the time function $(T + \Delta T)/\Delta T$ (Horner, 1951).

3.4. Slip and Dilation Tendency Analysis

To determine the likelihood of fault reactivation, we used the observed fault geometries combined with the estimated stress states to compute the slip and dilation tendency (Morris et al., 1996; Worum et al., 2004). Slip tendency (T_s) is the ratio of shear stress (τ) to normal stress (σ_n) acting on a fault. For slip to occur on a cohesionless fault (i.e., reactivation of a Byerlee material), the resolved shear stress must be equal to or greater than the frictional resistance to sliding, governed by the coefficient of friction (Morris et al., 1996). In other words, if the slip tendency value exceeds the value of the coefficient of friction, slip will occur. Dilation tendency (T_d) is the likelihood for a fault or fracture to dilate based on the three-dimensional

stress conditions. Dilation tendency values range from 0 to 1 with higher values indicating a more optimal orientation for dilation. Slip and dilation tendency are defined by the following equations:

$$T_s = \tau/\sigma_n \quad (7)$$

$$T_d = (\sigma_1 - \sigma_n)/(\sigma_1 - \sigma_3) \quad (8)$$

Slip and dilation tendency analyses were completed on the modeled faults using 3DStress® (e.g., Morris et al., 1996; Worum et al., 2004). Along with the modeled faults, the orientation and magnitude for σ_1, σ_2, and σ_3 were input into 3DStress®. Slip and dilation tendency was calculated for individual fault planes and projected onto the fault surfaces. Because of uncertainties in the magnitude of SH_{max}, SS ($SH_{max} > S_v > Sh_{min}$) and normal-slip ($S_v > SH_{max} > Sh_{min}$) faulting states are possible. Slip and dilation tendency for both stress states in the Arbuckle and Mississippian were calculated based on the lowest and highest values of SH_{max} (equations (1) and (2)) and using the average estimated orientation of SH_{max} (075°). At basement depths, the magnitude of SH_{max} is based on frictional failure equilibrium assuming Andersonian faulting (Anderson, 1951), estimated from the boundaries of a stress polygon (Moos & Zoback, 1990; Zoback et al., 2003). The stress polygon reveals a possible range of SH_{max} and Sh_{min} values consistent with a SS stress state. Therefore, the analysis was completed using intermediate magnitudes for both SH_{max} and Sh_{min}. Results were then compared to results using the highest and lowest possible magnitudes for both. For a NS stress state, an intermediate value for SH_{max} was used. Slip and dilation tendency estimates were completed using the measured stress state at Mississippian (1.12 km) and Arbuckle (1.48 km) depths, as well as the estimated stress state at a basement depth of 5.85 km, the average depth of induced events in Kansas reported by the NEIC.

In addition to evaluating the likelihood of failure using the above approach, we evaluated the fault geometries in Mohr space to determine the sensitivity to failure due to changes in pore fluid pressure. By forward modeling the pore fluid pressures required for failure, we determined a critical pressure threshold for each fault. For our study, we assume a μ of 0.6 and compared this with a more conservative estimate using μ of 0.5 (Byerlee, 1978). Additionally, we evaluated pore fluid pressure changes for SS and NS stress states at depths in the Mississippian, Arbuckle, and basement. We also conducted sensitivity analyses to evaluate the effects of stress orientation and magnitude to better quantify uncertainties in slip tendency calculations.

4. Results

4.1. Fault Geometry

Within the 3-D data set for the Wellington and Anson Bates fields, we identified 12 mostly vertical faults, striking between 325° and 049°, with the majority of the faults striking NNE (Figures 4 and 5) (Table 1). By comparison, naturally occurring conductive fractures identified in image logs from wells KGS 1–28 (N = 12) and KGS 1–32 (N = 12) have similar orientations, with the majority ranging from 20° to 40° and 10° to 20°, respectively (Figure 6). The NNE striking faults are consistent with the NNE trending Nemaha uplift, Humboldt fault zone, and Midcontinent Rift system, as well as with nodal planes from moment tensor solutions for recent earthquakes in south central Kansas and northern Oklahoma (Figure 1). The majority of the faults cut both the Mississippian and Arbuckle. Although the data quality is diminished near the base of the Arbuckle, several faults were observed cutting the top of the crystalline basement as well (faults 1, 2, and 3). Only one fault (9) fails to cut the Arbuckle and is contained within the Mississippian formation.

Faults were measured with lengths (strike dimension) ranging from 210 to 4,450+ m, widths (dip dimension) between 62 and 990+ m, and vertical separation between 12 and 33 m (Table 1). At least three of the faults (1, 2, and 3) extend beyond the boundaries of the 3-D seismic volume and vertically below the base of the Arbuckle (Figure 5), suggesting that they are likely longer and deeper than our measurements, which should be considered when evaluating the seismic hazard associated with these structures. The largest of the mapped faults is at least 4,450 m in length, at least 883 m in width and has 22 m of vertical separation. Fault length area-scaling relationships suggest the structure has the potential for a M5.8+ earthquake, although it is unlikely that the entire fault would reactivate during a single event (Hanks & Bakun, 2008; Wells & Coppersmith, 1994). However, this magnitude estimate of may not be entirely accurate because the full extent of the fault is unknown.

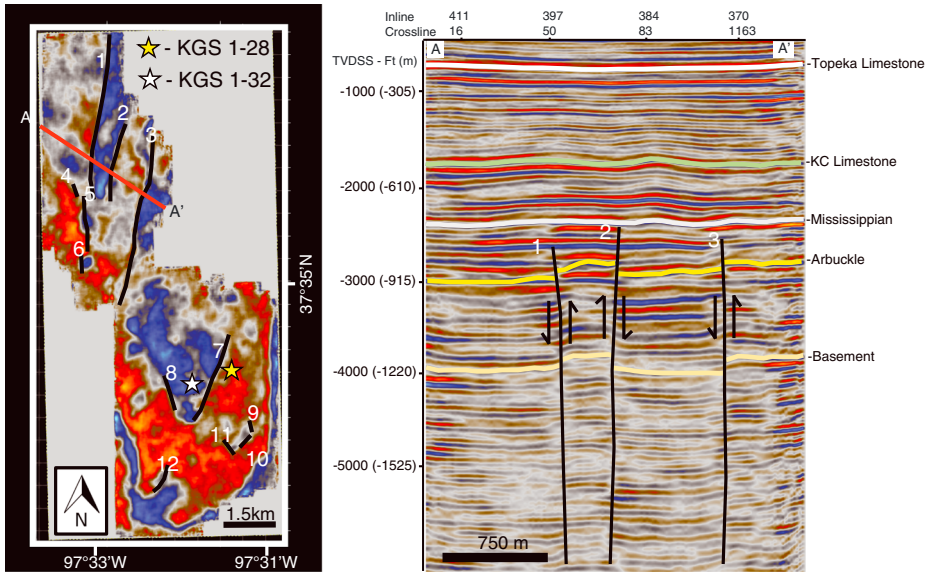

Figure 4. (left) Map view of study area with projected fault planes (solid lines). The depth slice was taken at the top of the Arbuckle at −871 m (TVDSS) and shows amplitude highs (red) and lows (blue), including areas of abrupt amplitude change, representing potential faults. Fault 7 is in close proximity to the injection wells and is at the highest risk for reactivation. (right) Vertical seismic profile (A-A′; 3 times vertical exaggeration) showing amplitude highs (red) and lows (blue), with mapped faults 1, 2, and 3, and slip direction, as well as mapped stratigraphic horizons. Faults were mapped by identifying offsetting stratigraphic horizons and breaks in amplitude. The top of the Mississippian, Kansas City Limestone, and Topeka Limestone were not cut by the underlying faults. Faults 1, 2, and 3 clearly cut the top basement reflector and appear to continue beyond the boundaries of the data.

4.2. Stress Orientations and Magnitudes

The orientation of SH_{max} was estimated by measuring the orientation of 40 drilling-induced tensile fractures from wells KGS 1–28 (N = 5), KGS 1–32 (N = 5), McGrath 1–16 (N = 15), and Spriggs 1–34 (N = 15) (Figure 1). The majority of induced fractures were centerline fractures (N = 32); however, petal fractures were also recorded (N = 8). Fractures range in height between 200 m and 1 m, with the majority below 30 m (Table 2). Based on the criteria established by Zoback and Zoback (1991), wells KGS 1–28, KGS 1–32, and McGrath 1–16 are graded C and well Spriggs 1–34 is graded B (Table 2). The relatively low grades are based on small sample size and widths of the fractures. Fracture orientations range from 055° to 087°, with an

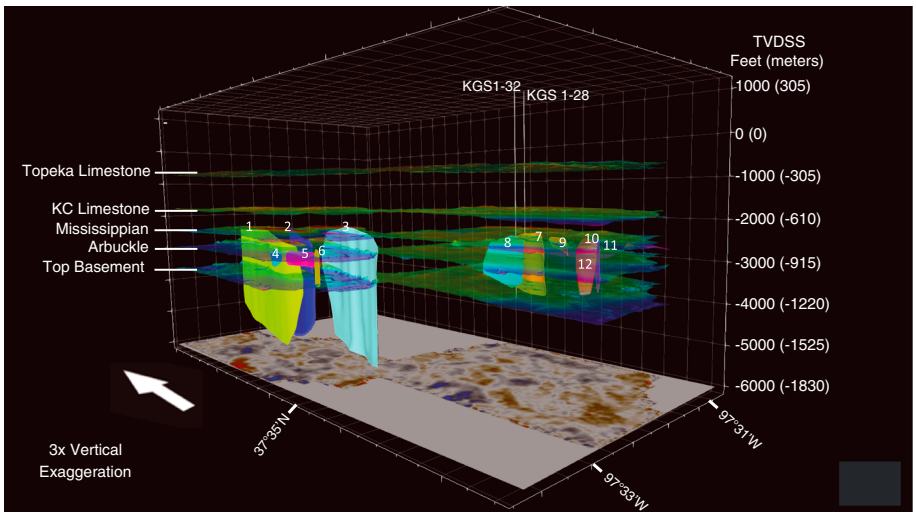

Figure 5. Three-dimensional model of the study area looking to the NE. The model shows the location and geometry of 12 subsurface faults, 5 major mapped stratigraphic horizons, and the KGS 1–28 and KGS 1–32 wells (3 times vertical exaggeration). Faults are oriented approximately NNE (Table 1). The majority of faults, excluding fault 9, terminate at the top of the Mississippian and cut the Arbuckle. Although seismic data quality diminishes below the Arbuckle, faults 1, 2, and 3 clearly cut the top basement reflector and could be potential pathways for fluid flow to greater depths.

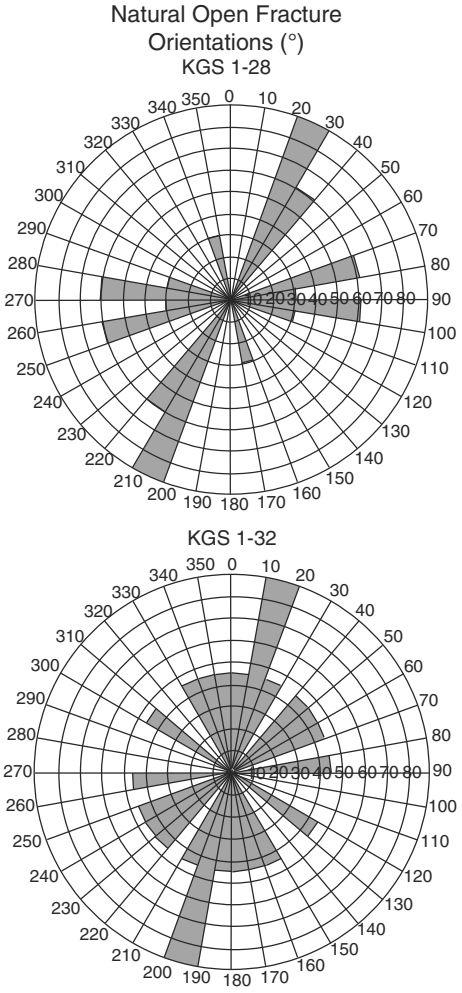

Figure 6. Natural open fracture orientations at KGS 1–28 (N = 12) at depths of 924–1,600 m and KGS 1–32 (N = 12) at depths of 1,075–1,597 m. Fracture orientations vary, with the majority ranging from 010° to 040°. This range in azimuth is consistent with optimally oriented faults in the study area and suggests that the modeled faults could also be conductive.

average of 077° and standard deviation of 007° (Figure 7). Measurements of the drilling-induced tensile fractures for KGS 1–28 and KGS 1–32 were originally completed by Haliburton and are consistent with the measurements taken for this study (Figure 8).

Inversion of SS (N = 36) and NS (N = 30) moment tensor solutions provides a best fit stress state with an average SH_{max} oriented ~075°. There do not appear to be any local trends in nodal plane orientation or sense of slip in the sample area, suggesting that the stress state is consistent across the study area (Figure 1). The estimates from SS (SH_{max} = 080°) and NS (SH_{max} = 070°) moment tensors were processed separately with 2,000 repetitions each to increase confidence to around 95% (Michael, 1987) (Figure 9). These results are consistent with detailed stress analyses in Oklahoma that also suggest an SH_{max} oriented ENE for both SS and NS moment tensor solutions (Alt & Zoback, 2015; Dart, 1990; Holland, 2013).

Stress magnitudes for S_v (36.6 MPa), Sh_{min} (18.4 MPa), and SH_{max} (31.3–45.9 MPa) were estimated at a depth of 1,484 m within the Arbuckle formation. Stress gradients (S_v = 24 MPa/km; Sh_{min} = 12.4 MPa/km; SH_{max} = 21–31 MPa/km), shown in Figure 10, are based on the calculated stress magnitudes at gauge depth. The range and uncertainty in SH_{max}, which overlaps values of S_v, suggests that both SS ($Sh_{max} > S_v > Sh_{min}$) and NS ($S_v > SH_{max} > Sh_{min}$) faulting are possible, consistent with the observed SS and NS moment tensor solutions for earthquake across the region. The pore fluid pressure at 1,484 m is 14.5 MPa based on the pump test from the KGS 1–32 well. For Mississippian depth (1,120 m), stress magnitudes were estimated at S_v (27 MPa), Sh_{min} (14 Mpa), and SH_{max} (23–34 MPa) using the stress gradients shown in Figure 10.

At basement depth (5.85 km), the estimated Sv is 155.3 MPa and is used to construct a stress polygon for a coefficient of friction of 0.6 (Figure 11). The boundaries of the stress polygon indicate the possible range of SH_{max} and Sh_{min} magnitudes at failure. For a SS stress state, an intermediate estimate using a midrange value for SH_{max} (201 MPa) and Sh_{min} (103 MPa) is used for slip tendency analysis. Results were then compared to the highest (SH_{max} = 363 MPa; Sh_{min} = 155 MPa) and lowest (SH_{max} = 155 MPa; Sh_{min} = 89 MPa) possible stress value combinations for a SS stress state. For a NS stress state, slip tendency analysis uses stress values at failure equilibrium with an intermediate value for SH_{max} (138 MPa).

4.3. Potential for Fault Reactivation

Results from the slip tendency analysis for the observed faults in the Mississippian reservoir are shown in Figure 12 for an SH_{max} oriented 075°. We estimate the stress state S_v (27 MPa), Sh_{min} (14 MPa), and SH_{max} (23–34 MPa) using the stress gradients calculated at the injection interval (1,116 to 1,129 m). The highest and lowest values of SH_{max} for SS (34 MPa) and NS (23 MPa) stress states were used in the final slip tendency analysis. For a SS stress state, slip tendency values ranged from 0.46 to 0.01. By projecting fault planes into Mohr space, we estimate the critical pore fluid pressure that would promote failure. At Mississippian depth, optimally oriented faults would require an additional pore fluid pressure of 1.1 MPa (μ = 0.5) to 4.13 MPa (μ = 0.6) to induce favorable conditions for failure on faults in a SS stress state (SH_{max} = 34 MPa) (Figure 13). Based on the stress field, faults were determined to be poorly to optimally oriented for failure in a SS stress state, with the majority of faults being moderately oriented for failure. In a NS stress state (SH_{max} = 23 MPa), slip tendency values were less than 0.34 with a required pore fluid pressure change of 5.79 MPa (μ = 0.5) to 7.6 MPa (μ = 0.6) to reach failure on optimally oriented faults (Figure 13). Faults are mostly moderately to

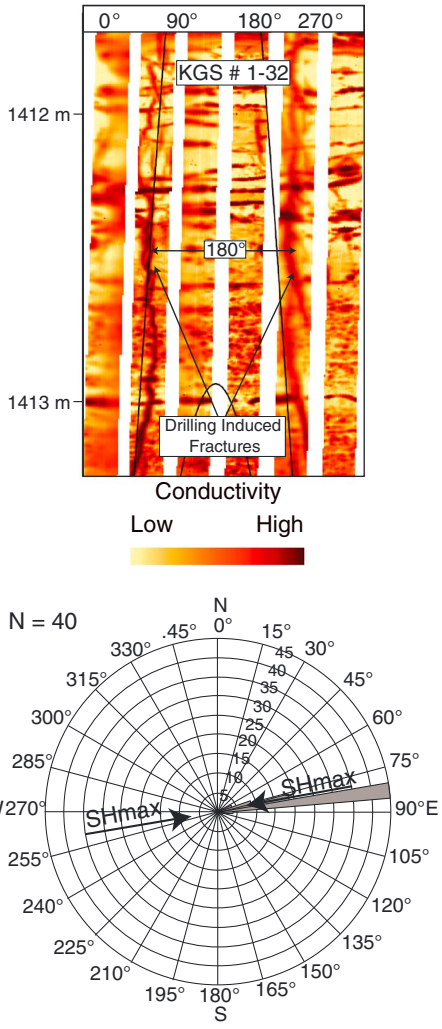

Figure 7. (top) Image log from well 1–32 generated through microresistivity measurements of low conductivity (bright) and high conductivity (dark) areas. Drilling-induced tensile fractures are identified from image logs as highly conductive features running vertically along the wellbore wall with 180° separation. Drilling-induced fractures are consistent with the maximum horizontal stress (SH_{max}) direction. (bottom) Rose diagram of 40 drilling-induced tensile fractures, based on 80 total measurements taken from four wells in south central Kansas. SH_{max} measurements ranged from 055° to 087° with an average of 077° and a standard deviation of 007°.

poorly oriented for failure in a NS stress state. Dilation tendency within the Mississippian is low overall, with most fault planes having dilation tendency values less than 0.3. Due to high differential stresses, slip is much more likely.

The results from the slip tendency analysis for faults in the Arbuckle reservoir are shown in Figure 13 for an SH_{max} oriented 075°. Stress magnitudes at the Arbuckle reservoir depth of 1,484 m is calculated for S_v (36.6 MPa), Sh_{min} (18.4 MPa), and SH_{max} (31.3–45.9 MPa). In a SS stress state, assuming the highest estimated value for SH_{max} (45.9 MPa), slip tendency reached values up to 0.47 (Figure 13). Depending on the fault zone properties, in order for optimally oriented faults to reach failure, an increase in pore fluid pressure of 1.31 MPa (μ = 0.5) to 5.37 MPa (μ = 0.6) is required (Figure 13). In a NS stress state (SH_{max} = 31.3 MPa), slip tendency values reached up to 0.35 (Figure 13). An increase in pore fluid pressure of 7.0 MPa (μ = 0.5) to 9.8 MPa (μ = 0.6) is required to reach failure conditions for optimally oriented faults (Figure 13). Dilation tendency values within the Arbuckle are also low, with most fault planes having dilation tendency values less than 0.2.

Slip tendency analysis at basement depth for a SH_{max} oriented 075° was also conducted using a stress polygon, assuming Andersonian faults in failure equilibrium (e.g., Moos & Zoback, 1990; Zoback et al., 2003). Due to limitations of the seismic data, which prevented mapping of faults at deeper basement depths, shallow faults were projected to 5.85 km, the average depth of NEIC-reported injection-induced earthquakes in south central Kansas. Assuming a SS stress state, the slip tendency analysis demonstrates that portions of two faults (7 and 10) would be at failure and likely to slip in response to very small pore fluid pressure changes, three of the faults (2, 3, and 12) would slip in response to pore fluid pressure changes greater than 3.4 MPa, and the remaining seven faults (1, 4, 5, 6, 8, 9, and 11) were unlikely to fail under the presumed stress state, requiring a change in pore fluid pressure of 13 MPa or more to reach failure (Figure 13). Furthermore, in a NS stress state, none of the faults are near failure, five faults (2, 3, 7, 10, and 12) would slip with a pore fluid pressure increase of 5.4 MPa or more, and the remaining seven faults (1, 4, 5, 6, 8, 9, and 11) were less likely to fail, requiring a change in pore fluid pressure of 14.5 MPa or more (Figure 13).

Uncertainties associated with the stress polygon estimations indicate a possible range of SH_{max} and Sh_{min} values (Figure 11). When compared to the intermediate analysis, slip tendency analysis using the highest values of SH_{max} (363 MPa) and Sh_{min} (155 MPa) for a SS stress state brings additional faults to failure, including areas of faults 1, 7, and 12 and the entirety of fault 10. Conversely, faults are less likely to slip using lower values of SH_{max} (155 MPa) and Sh_{min} (89 MPa), with only a small portion of fault 12 reaching failure conditions. Considering the occurrence of induced events to the west and south indicating a critical stress state, and the presence of both SS and NS moment tensor solutions indicating similar magnitudes for SH_{max} and S_v, it is likely that the intermediate estimates (Figure 13) more closely represent the actual stress state at basement depth.

5. Discussion

5.1. Potential for Fault Reactivation Within the Mississippian and Arbuckle Reservoirs

Based on the mapped fault orientations and geometries, the relationship of the faults to the estimated stress field, and the volume of CO_2 planned for injection (40,000 t per well), the faults in the study area appear to be

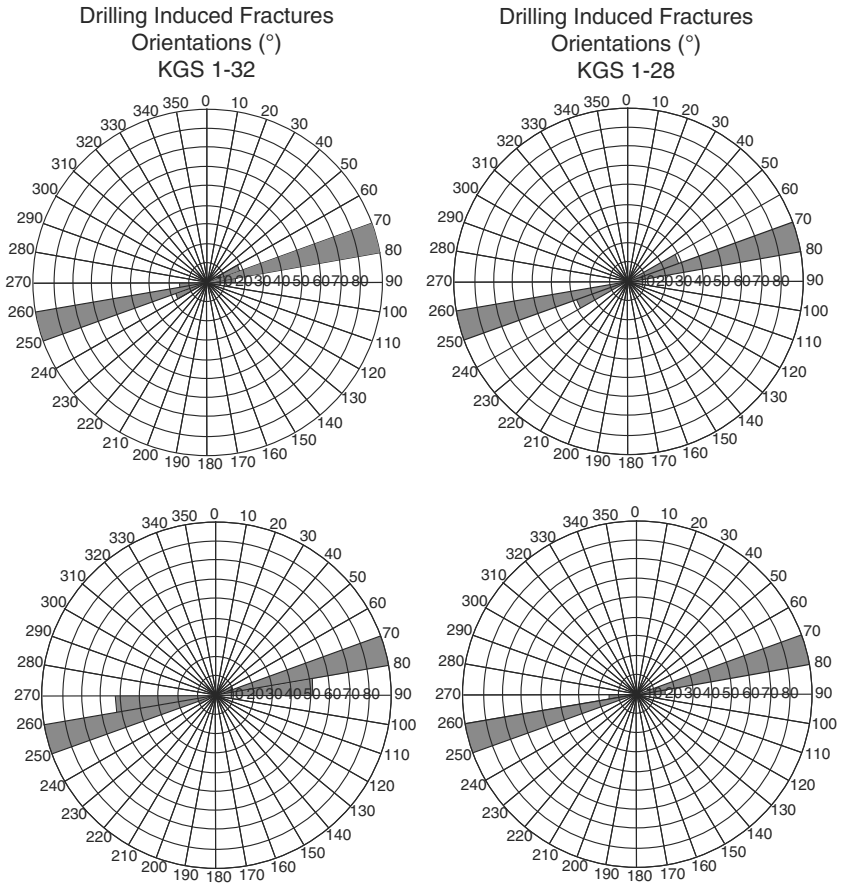

Figure 8. Rose diagrams of drilling-induced tensile fractures measured by Haliburton for (left column) well KGS 1–32, at depths of 1,075–1,596 m (top; $N = 132$) and 683–1,075 m (bottom; $N = 29$), and for (right column) well KGS 1–28 (right), at depths of 923–1,600 m (top; $N = 99$) and 671–923 m (bottom; $N = 15$). SH_{max} orientation ranged between 073° and 076°, consistent with measurements taken by this study.

stable at reservoir depths (Mississippian: 1,116–1,129 m; Arbuckle: 1,496–1,539 m). Fault strikes range between 325° and 049°. Relative to our estimates of the stress field, an optimally oriented fault would strike between 035° and 057° in a SS stress state and normal faults would strike between 066° and 092°. These values are consistent with observed nodal planes from earthquake moment tensor solutions, which ranged between

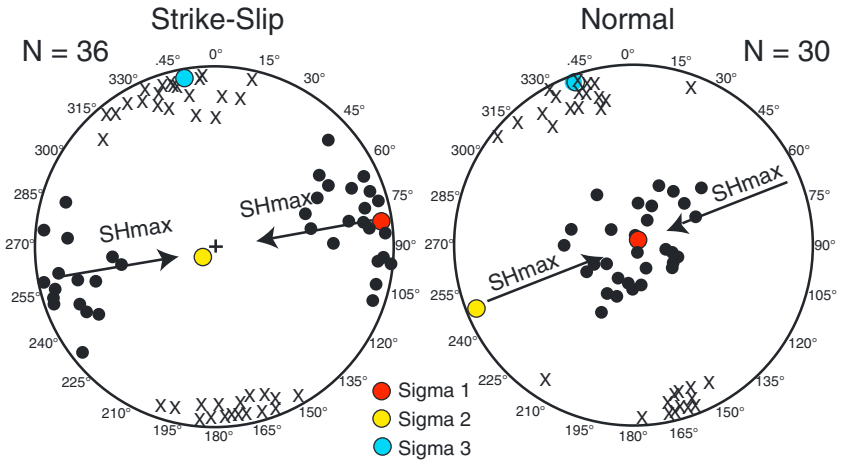

Figure 9. Results of stress inversion of earthquake moment tensor solutions. Data were collected from the NEIC ANSS catalog from south central Kansas and north central Oklahoma from January 2012 to April 2016. Both strike-slip ($n = 36$) and normal-slip ($n = 30$) moment tensor solutions were collected and were inverted separately. Average estimate for SH_{max} ranged from 080° (SS) to 070° (NS) with an overall average of ~075°. Plots were created using STRESSInverse (Vavryčuk, 2014) software based on the method proposed by Michael (1984, 1987).

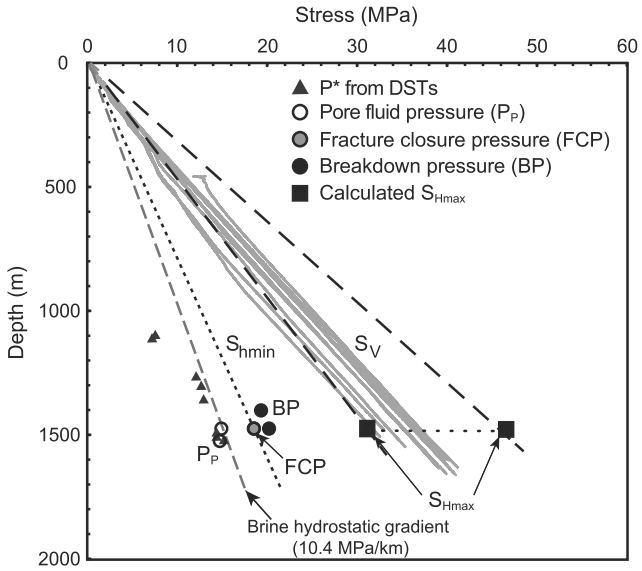

Figure 10. Stress gradients based on density logs, step rate, and drill stem tests, and calculations of SH_{max} following Zoback et al. (2003). Fracture closure pressure, the best estimate for the magnitude of Sh_{min}, was determined from a pump test in KGS 1–32 at gauge depth of 1,484 m. Pore fluid pressure estimates from several sources are shown and can be compared to hydrostatic gradient for brine (10.4 MPa/km).

000° and 064° (SS) and 038° and 105° (NS) (Figure 9). Although two of the mapped faults (7 and 10) fall within the range of optimal orientation for a SS stress regime, the majority are only moderately (2, 3, and 12) to poorly (1, 4, 5, 6, 8, 9, and 11) aligned for reactivation, as demonstrated by the slip tendency analysis, shown in Figure 13.

Although the orientations of at least two of the mapped faults suggest risk for reactivation, further analysis reveals that even the most susceptible faults, including fault 7 which is in close proximity to the injection wells (0.25 km), would require a pore fluid pressure increase in excess of that anticipated with pilot-scale injection to initiate failure (Figure 13). Maximum pressure changes associated with the planned CO_2 injection activities at Wellington Field were determined through numerical multi-phase flow simulations for the Mississippian and Arbuckle reservoirs (Holubnyak et al., 2016). The models, which incorporate well log and test data, 3-D seismic reflection data, and a host of other reservoir parameters (e.g., temperature, fluid properties, relative permeability, and capillary pressure), suggest that after 9 months of injection into the Arbuckle, the estimated pore fluid pressure change would be 0.4 MPa at the borehole and $<$0.15 MPa at distances of 150 m or greater from the wellbore (Holubnyak et al., 2016). By comparison, the slip tendency analysis shows that under a likely coefficient of friction (μ = 0.6) and the highest risk stress state (SS), an order of magnitude increase in pore fluid pressure is required to reach failure at reservoir conditions (4.13 MPa at Mississippian; 5.37 MPa at Arbuckle). This result holds true even when a more conservative coefficient of friction (μ = 0.5) is used (1.1 MPa at Mississippian; 1.31 MPa at Arbuckle). In a NS stress state, the slip tendency would be lower, requiring an even greater change in pore fluid pressure to induce failure.

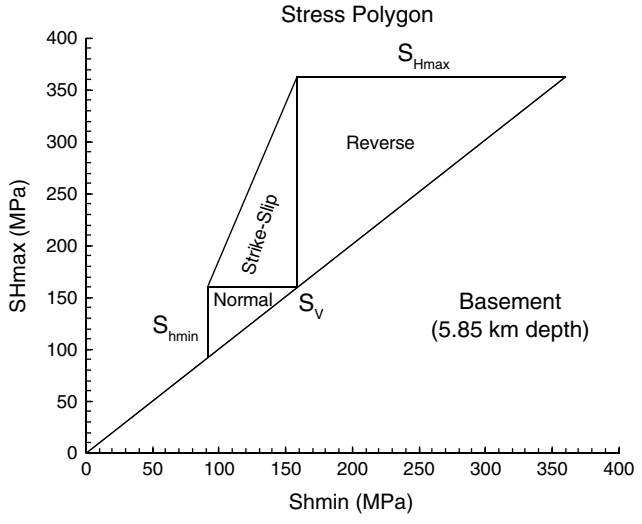

Figure 11. Stress polygon showing possible stress magnitudes for SHmax and Shmin for different stress environments (strike-slip, normal, and reverse) for an estimated Sv magnitude of 155 MPa. Estimates were made for a depth of 5.85 km, the average depth of NEIC-reported induced events in south central Kansas. Polygon boundaries represent a state of failure for optimally oriented faults. For a strike-slip stress state, an intermediate value for SH_{max} and Sh_{min} was used for the slip tendency analysis. For a normal slip stress state, an intermediate value for SH_{max} was used for the slip tendency analysis.

Uncertainties in stress orientations and magnitudes can significantly impact the slip tendency analysis results. The most significant uncertainties are associated with the magnitudes of the horizontal stresses. Sh_{min} is only constrained by three recorded pressures, all within the Arbuckle. At gauge depth (1,484 m), sensitivity tests suggest that a 10% reduction in the magnitude of Sh_{min} would increase slip tendency by 12% (from 0.47 to 0.53) for a SS stress state, and 16% (from 0.35 to 0.41) for a NS stress state (Figure 14). Uncertainties in these values also affect SH_{max}, which is reliant on accurate estimates for Sh_{min}. Similarly, the orientation of SH_{max}, which has a range of potential values, also introduces some uncertainty into the analysis (Figures 7 and 9). For example, a more northerly azimuth of SH_{max}, assuming a SS stress state, would result in more fault planes moving into favorable orientations. Conversely, a more easterly azimuth of SH_{max} (081°) removes any faults from optimal orientation.

Based on the slip tendency analysis and associated uncertainties, it seems reasonable to conclude that the mass of CO_2 planned for injection is unlikely to reactivate the observed faults at reservoir conditions. The suitability of the Arbuckle and Mississippian for fluid injection is due in part to the naturally underpressured nature of the reservoirs. For the Mississippian, underpressured conditions are further enhanced by pressure depletion due to oil production (e.g., Bachu, 2000; Keranen et al., 2013; Puckette & Al-Shaieb, 2003). Furthermore, the Mississippian is undergoing repressurization.

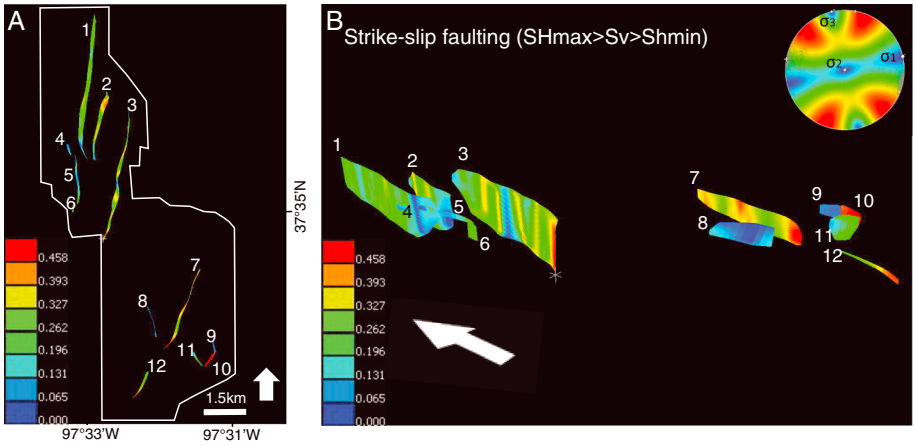

Figure 12. Slip tendency analysis for faults at Mississippian depth (1,120 m) in a strike-slip stress state. Slip tendency values are projected on to the modeled faults (A and B) and show that the majority of faults are stable with only some faults with areas that are optimally oriented for failure.

Injection volumes have surpassed 20,000 t of CO_2 at a rate of 100–150 t/d, with pore fluid pressures at near hydrostatic (11 MPa) (Holubnyak et al., 2016). Currently, there is no occurrence of induced seismicity in response to repressurization of the reservoir.

5.2. Potential for Fault Reactivation Within Precambrian Basement

Our analysis shows there is a low likelihood of reactivating faults within the Mississippian and Arbuckle—a conclusion supported by earthquake hypocenters in the region, the vast majority of which are located at 3–7 km depth, well below these reservoirs. Thus, the primary concern for the study area is reactivating basement faults. One of the most significant findings in this study is the identification of faults cutting the Arbuckle and Precambrian basement. These faults may provide hydraulic connections or pressure pathways between the Arbuckle and basement (e.g., Zhang et al., 2013). Image log analysis from wells KGS 1–28 and KGS 1–32 reveal a number of natural conductive fractures, some of which reach depths of at least 1,600 m, well into the basement rock. Orientations of these natural open fractures vary, with the majority striking between 010° and 040°, consistent with the mapped fault orientations (Table 1 and Figure 6). Conductive faults paired with the lack of a seal between the Arbuckle and basement are concerning, as both are reported to have a significant effect on the occurrence of induced seismicity in basement rock (Barton et al., 1995; Morris et al., 2011; Zhang et al., 2013). Elevated pore fluid pressures could propagate downward along distributed fracture networks into the Precambrian crystalline basement, suggesting that slip tendency analysis at reservoir depths and conditions may not be adequate for characterizing the risk of induced seismicity associated with fluid injection. This also highlights the importance of slip tendency analysis at basement depths, which shows that faults, like those mapped in the field, are in failure equilibrium at 5–6 km.

If the faults at basement depth are critically stressed and in failure equilibrium, as suggested by this study and others (e.g., Townend & Zoback, 2000; Zoback & Gorelick, 2012), it is possible that even small pore fluid pressure changes (0.01 to 0.1 MPa) could induce failure (Reasenberg & Simpson, 1992; Seeber & Armbruster, 2000; Stein, 1999; Zoback & Gorelick, 2012). For example, the critical threshold for failure associated with the injection-induced earthquake swarm in Jones, Oklahoma, was reported by Keranen et al. (2013) and Keranen et al. (2014) to be 0.07 MPa. The results of our basement analysis show that several of the mapped faults, when projected to basement depth, would be in failure equilibrium, likely to fail in response to very small pore fluid pressure changes. However, when considering the earthquake potential of faults in our study area, it is important to note that only small portions of these faults would be in favorable orientations. For instance, for fault 7, only about one tenth of the fault area is optimally oriented, and although failure could occur in these areas under minor pore fluid pressure increases, a change in pore fluid pressure of over 35 MPa would be required to reactivate the entirety of the fault. Such a scenario, while unlikely, could result in a magnitude 5.5 event (Hanks & Bakun, 2008; Wells & Coppersmith, 1994).

Although the slip tendency analysis we have performed provides an estimate of the likelihood of fault reactivation, there are limitations to our analysis. The analysis only accounts for mapped faults. Several of the

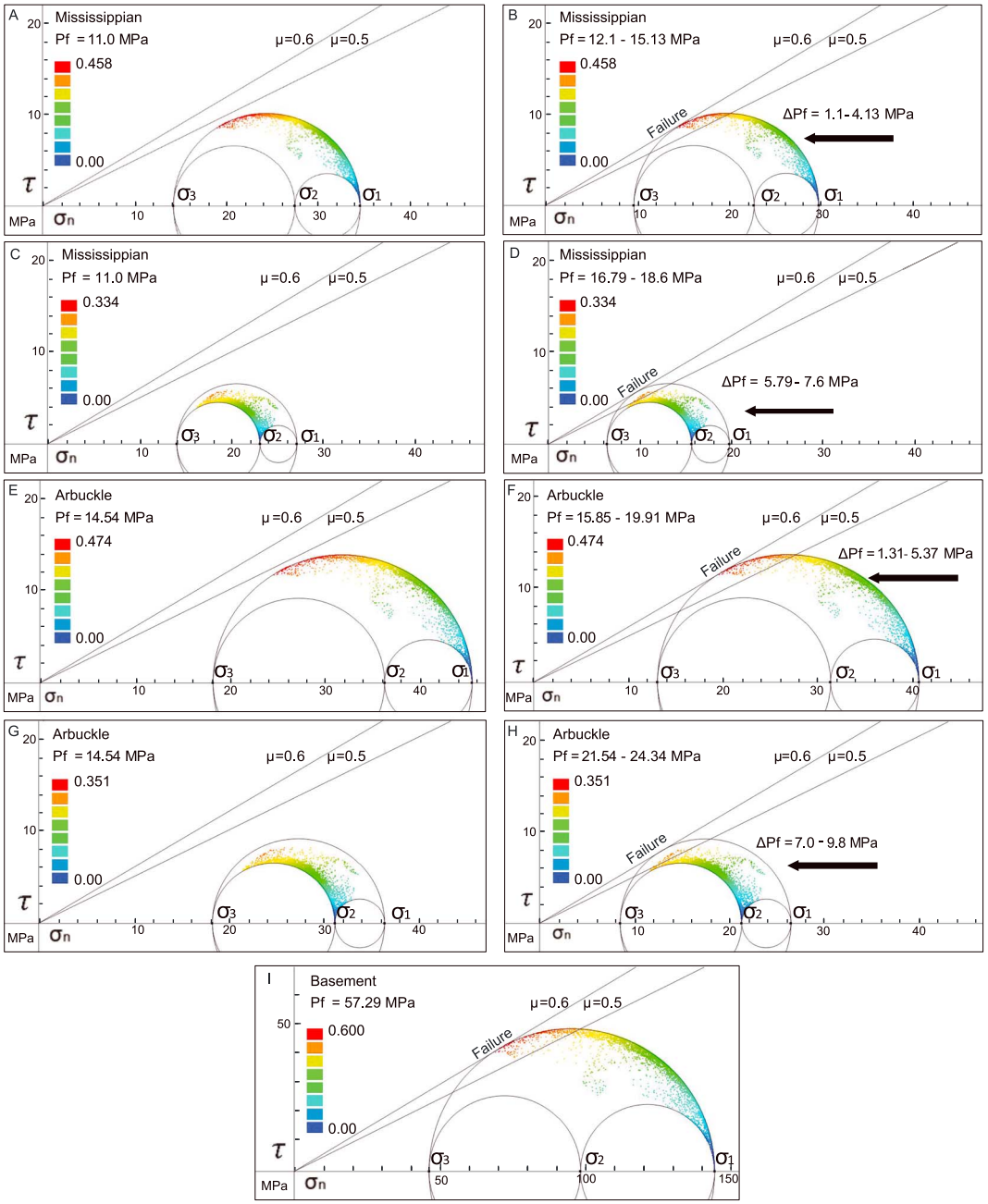

Figure 13. Slip tendency analysis for faults at (a–d) Mississippian depth (1,120 m), (e–h) Arbuckle depth (1,484 m), and (i) basement depth (5,850 m) for SS (Figures 13a and 13b, 13e and 13f, and 13i) and NS (Figures 13c and 13d, and 13g and 13h) stress states. Fault planes were projected into Mohr circle space with failure envelopes for coefficient of friction of 0.5 and 0.6. For each scenario, pore fluid pressure was increased until failure was reached. At basement depth, a number of faults are already at failure for the estimated stress state.

documented faults extend beyond the limits of the seismic data and thus could be in different orientations in those areas. The analysis also assumes that the mapped structures are representative of structures in the deep basement. The basement could contain faults in orientations not represented by our analysis. Many of the recent moderate magnitude injection-induced earthquake in Oklahoma, like the *M*5.8 Pawnee and *M*5.0 Cushings earthquakes, have occurred on such unmapped structures (McNamara et al., 2015; Yeck et al., 2016, 2017). Our analysis is also independent of other parameters that could increase or decrease the likelihood of fault reactivation. The slip history and associated earthquake cycle effects could alter the likelihood for slip on a given fault. The hydraulic properties of the basements rocks and faults could also

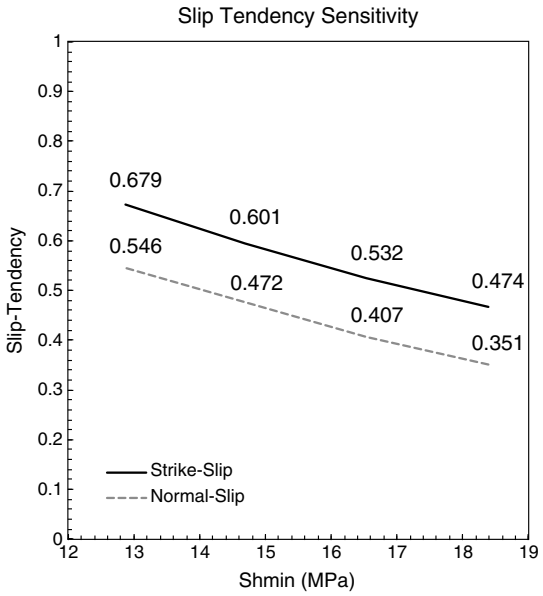

Figure 14. Slip tendency uncertainty was calculated for measurements taken at Arbuckle depth (1,484 m) for both SS and NS stress states. Sh_{min} was reduced by 10%, 20%, and 30%, and the resulting slip tendency was recorded. Results showed that slip tendency increases with reduced magnitudes of Sh_{min}.

promote or hinder failure on particular structure. Coulomb stress changes, associated with individual earthquakes, are also unaccounted for in our analysis.

5.3. Implications for Fluid Disposal and CO_2 Sequestration

Thus far, our study has addressed concerns associated with pilot-scale injection of CO_2, (~40,000 t; 438,000 barrels (bbl) brine equivalent), with a proposed injection rate of approximately 50,000 bbl/m. In order to have a significant impact on the volume of CO_2 or brine generated through human activity, fluid injection must operate on a massive scale (e.g., Zoback & Gorelick, 2012) and could require the implementation of a large number of high-rate injection wells. Recent seismicity in the region suggests there are challenges associated with large-scale fluid disposal, particularly when high rates of injection are considered. Weingarten et al. (2015) showed that seismicity across the U.S. midcontinent over the past 7 years strongly correlates with the development of high-rate injection wells (>300,000 barrels per month) compared to other factors like cumulative injected volume (McGarr, 1976; McGarr, 2014), proximity to basement (Kim, 2013; Zhang et al., 2013), or wellhead pressure (Frohlich, 2012; Keranen et al., 2014). The correlation between high-rate injection and seismicity is consistent with the fluid disposal and earthquake histories of Harper and Sumner counties, where brine disposal in the Arbuckle Group had operated for decades without significant issue. Prior to 2012, average injection rates per well were 16,500 bbl/m, with the highest single well injection rate reaching 83,333 bbl/m in 2008. Statewide seismicity occurred at a rate of one to two earthquakes per year from 1977 to 2012 (Buchanan, 2015; Hildebrand et al., 1988; see Acknowledgments and Data). Between 2012 and 2014, average injection rates per well rose to 41,140 bbl/m, with the highest single well injection rate reaching 704,471 bbl/m in 2014. A concomitant increase in seismicity has been observed in these counties where more than 1,000 *M*2.0+ events have occurred since 2014, the majority of which have been near high-rate wastewater disposal wells (Figure 2) (see Buchanan, 2015 and Acknowledgments and Data).

When considering the injection of CO_2 in areas susceptible to earthquakes, the possibility of damaging seals and causing leakage into overlying strata and underground freshwater aquifers is a major concern (e.g., Benson & Cole, 2008; Chiaramonte et al., 2015; Morris et al., 2010; Streit & Hillis, 2004; Vilarrasa et al., 2014). CO_2 is less dense and more buoyant than in situ fluids and therefore rises to the base of overlying seals. Fracture reactivation through small to moderate earthquakes could damage the integrity of the seals and allow CO_2 to migrate into shallower layers or even escape to the surface, releasing CO_2 back into the atmosphere (Shipton et al., 2006; Zoback & Gorelick, 2012). A *M*4.0 event, for instance, could be associated with several millimeters to centimters of slip along a fault (Cappa & Rutqvist, 2011; Stein & Wysession, 2009), enough to create hydraulic pathways that could compromise seal integrity and allow for CO_2 to escape.

The Chattanooga Shale, which is the primary seal for the Arbuckle Group, is extensive across the region, with thicknesses between 1 and 50 m (Goebel, 1968; Lee, 1940; Zeller, 1968). There are also a number of shallower secondary seals could mitigate risks if the primary seal was compromised (Goebel, 1968; Lee, 1940; Zeller, 1968). The adequacy of these seals is suggested by the pressure conditions of the Arbuckle and Mississippian reservoirs, which are below hydrostatic across much of the region, an indication that pressures have not equalized over geologic timescales or during past earthquakes (Nelson & Gianoutsos, 2011; Sorenson, 2005).

5.4. Mitigation Strategies

Although safe fluid injection into the Arbuckle is possible, the increasing demand for fluid disposal highlights the need for alternative injection sites and alternative uses of these fluids. One possibility is injection into depleted oil and gas reservoirs such as the Mississippian for waterfloods, EOR, and long-term storage.

Results from this study, along with the recent CO_2 injection test at Wellington Field, suggest that the Mississippian may be an adequate reservoir for secondary and tertiary recovery or for disposal of brine and/or CO_2. The Mississippian had been drawn down to approximately 6.2 MPa at Wellington Field due to oil and gas production (Holubnyak et al., 2016) and local repressurization operations have raised the pore fluid pressure to near hydrostatic (11 MPa) without any associated seismicity (W. L. Watney, personal communication, 2016). Depleted oil fields such as the Mississippian are located throughout the midcontinent. It is estimated that oil fields in Kansas alone have ~ 750 million barrels of CO_2-EOR recovery potential and are capable of accommodating 240–370 million tons of CO_2 (Midwest Governors Association and Great Plains Institute, 2012). Waterflooding operations into the Mississippian have also proved successful. For example, the neighboring Lee and Anson Bates fields in Sumner County achieved significant production increases in response to waterflood operations, which began in the early 1980s and without any associated seismicity (Bhattacharya et al., 2003).

Implementation of disposal or secondary and tertiary recovery methods into the Mississippian or similar reservoirs could face a number of challenges. These methods require knowledge of compatibility of the injected fluid with connate waters and the reservoir. The fluid injected could interact with reservoir rock, causing a reaction that could change the porosity and/or permeability of the reservoir (Alexeev et al., 2015; Nasralla et al., 2015). Treatment of the injected fluid could also be required to reduce the risk of contamination, including the removal of undesirable chemicals and bacteria (Buckley et al., 1987). Implementation also requires significantly more in terms of reservoir management and surveillance compared to the operation of a typical saltwater disposal well. The interaction between the oil and water, for instance, could potentially increase or decrease the recovery efficiency, affecting production (Agbalaka et al., 2009; Melrose & Brandner, 1974; Morrow, 1990; Tang & Morrow, 1997). Reservoir performance indicators, such as breakthrough times and fluid ratios, and reservoir pressures must be carefully monitored (e.g., Baker, 1998; Grinestaff & Caffrey, 2000).

6. Conclusions

Three-dimensional seismic data from the Wellington and Anson Bates fields reveal 12 mostly vertical faults striking approximately NNE. These faults cut Paleozoic units below the top Mississippian reflector and, where image quality is good and faults can be confidently carried, also appear to cut the top of the Precambrian basement. When evaluated within the context of the known stress field—derived from image log analysis, inversion of moment tensor solutions from recent earthquakes across the region, and well test data—these faults appear to be stable at reservoir depths, particularly in the context of the planned small-scale CO_2 injection. Our conservative estimates (assuming SS faulting and $\mu = 0.5$) show that these faults would require pore fluid pressure changes in excess of those anticipated for the pilot project (1.1 MPa at Mississippian; 1.3 MPa at Arbuckle) to reactivate. This reservoir-based analysis, however, does not adequately address the potential for seismicity within the Precambrian basement. We show that these features are likely conductive and critically stressed and can reactivate with small pore fluid pressure changes, a result that is consistent with the recent increase in seismicity in the region (Townend & Zoback, 2000; Zoback, 1992; Zoback & Gorelick, 2012; Zoback et al., 2002; Zoback & Zoback, 1980). Thus, our analysis suggests that reservoir-based assessments may be inadequate for accurately estimating the risk of injection-induced seismicity, particularly where earthquakes are spatially decoupled from injection intervals.

Based on our results, we also suggest that it is unlikely that the small volume of CO_2 (40,000 t) to be injected into the Arbuckle would induce the pore fluid pressure changes needed for failure, as similar small-scale injection has operated safely in the past in these counties and across Kansas. Rather, seismicity in Wellington Field and elsewhere in the region is more apt to occur where there are dense clusters of high-rate disposal wells. Under these commercial-scale operations, high-rate injection into an aquifer not sealed from the basement paired with conductive faults appears to be a recipe for induced seismicity (Barton et al., 1995; Morris et al., 2011; Zhang et al., 2013; Weingarten et al., 2015). However, the combination of good primary and secondary seals may mitigate risks associated with potential leakage into overlying freshwater aquifers.

Lastly, the increasing need for safe disposal sites means that alternative reservoirs should be considered. We suggest that underpressured reservoirs such as the Mississippian could be used for disposal and secondary/tertiary recovery methods, which could reduce the volume of fluid injected into the Arbuckle.

To consider the Mississippian or other reservoirs for these purposes, the compatibility between produced brines and/or CO_2 with reservoir rocks, connate waters, and hydrocarbons would first need to be considered.

Acknowledgments and Data

This research was supported by the U.S. Geological Survey (USGS), Department of the Interior, under USGS award G16AP00022, and the U.S. Department of Energy-National Energy Technology Laboratory (DOE-NETL), under grant DEFE0002056. The DEFE0002056 project is managed and administered by the Kansas Geological Survey and funded by DOE-NETL and cost-sharing partners. We are grateful to W. Lynn Watney, principal investigator for DEFE0002056, for including us in the Wellington Field study and providing us access to the various data sets we have used. We also thank Dana Wreath and Berexco, LLC, our industry partner on this study. We acknowledge M. FazelAlavi for assistance with density log and well test analyses, E. Holubnyak for support with reservoir engineering aspects of the study, J. Rush for assistance with Petrel, and J. Victorine for assistance with DST analyses. We would also like to acknowledge A. Morris for providing a license for and assistance with 3DStress® and Schlumberger for donating licenses for use of Petrel™. This manuscript benefited from thoughtful reviews by L. Stearns, and two anonymous reviewers. Earthquake data are available at the USGS Advanced National Seismic System (ANSS) comprehensive catalog (http://earthquake.usgs.gov/earthquakes/search/, last accessed April 2016). Class II saltwater disposal data were provided by the Kansas Corporation Commission (KCC; http://kcc.ks.gov, last accessed April 2016). The 3-D seismic reflection data used in the study are held by Citation Oil and Gas for Anson Bates Field and the Kansas Geological Survey for Wellington Field. Requests for academic use may be submitted to the Kansas Geological Survey at webadmin@kgs.ku.edu. This report was prepared as an account of work sponsored by an agency of the United States government. The United States government, any agency thereof, or any of its employees do not make any warranty, express or implied, or assume any legal liability or responsibility for the accuracy, completeness, or usefulness of any information, apparatus, product, or process disclosed, or represent that its use would not infringe privately owned rights. Reference herein to any specific commercial product, process, or service by trade name, trademark, manufacturer, or otherwise does not necessarily constitute or imply its endorsement, recommendation, or favoring by the United States government or any agency thereof. The views and opinions of authors expressed herein do not necessarily state or reflect those of the United States government or any agency thereof.

References

Aadnoy, B. S. (1990). In-situ stress directions from borehole fracture traces. *Journal of Petroleum Science and Engineering*, *4*(2), 143–153. https://doi.org/10.1016/0920-4105(90)90022-U

Agbalaka, C. C., Dandekar, A. Y., Patil, S. L., Khataniar, S., & Hemsath, J. R. (2009). Coreflooding studies to evaluate the impact of salinity and wettability on oil recovery efficiency. *Transport in Porous Media*, *76*(1), 77–94. https://doi.org/10.1007/s11242-008-9235-7

Alexeev, A., Shapiro, A., & Thomsen, K. (2015). Modeling of dissolution effects on waterflooding. *Transport in Porous Media*, *106*(3), 545–562. https://doi.org/10.1007/s11242-014-0413-5

Alt, R. C., and Zoback, M. D. (2015). A detailed Oklahoma stress map for induced seismicity mitigation. Paper presented at AAPG Annual Convention and Exhibition, Denver, CO.

Anderson, E. M. (1951). *The dynamics of faulting and dyke formation with applications to Britain*. Houston, TX: Hafner Pub. Co.

Angelier, J. (1979). Determination of the mean principal directions of stresses for a given fault population. *Tectonophysics*, *56*(3-4), T17–T26. https://doi.org/10.1016/0040-1951(79)90081-7

Argus, D. F., & Gordon, R. G. (1996). Tests of the rigid-plate hypothesis and bounds on intraplate deformation using geodetic data from very long baseline interferometry. *Journal of Geophysical Research*, *101*(B6), 13,555–13,572. https://doi.org/10.1029/95JB03775

Baars, D. L., & Watney, W. L. (1991). Paleotectonic control of reservoir facies. *Kansas Geological Survey Bulletin*, *233*, 253–262.

Bachu, S. (2000). Sequestration of CO_2 in geological media: Criteria and approach for site selection in response to climate change. *Energy Conversion and Management*, *41*(9), 953–970. https://doi.org/10.1016/S0196-8904(99)00149-1

Bahorich, M., & Farmer, S. (1995). 3-D seismic discontinuity for faults and stratigraphic features: The coherence cube. *The Leading Edge*, *14*(10), 1053–1058. https://doi.org/10.1190/1.1437077

Baker, R. (1998). Reservoir management for waterfloods—Part II. *Journal of Canadian Petroleum Technology*, *37*(1), 12–17.

Barton, C. A., Zoback, M. D., & Moos, D. (1995). Fluid flow along potentially active faults in crystalline rock. *Geology*, *23*(8), 683–686. https://doi.org/10.1130/0091-7613(1995)023%3C0683:FFAPAF%3E2.3.CO;2

Bell, J. S. (1990). Investigating stress regimes in sedimentary basins using information from oil industry wireline logs and drilling records. *Geological Society, London, Special Publications*, *48*(1), 305–325. https://doi.org/10.1144/GSL.SP.1990.048.01.26

Bell, J. S., & Gough, D. I. (1979). Northeast-southwest compressive stress in Alberta evidence from oil wells. *Earth and Planetary Science Letters*, *45*(2), 475–482. https://doi.org/10.1016/0012-821X(79)90146-8

Benson, S. M., & Cole, D. R. (2008). CO_2 sequestration in deep sedimentary formations. *Elements*, *4*(5), 325–331. https://doi.org/10.2113/gselements.4.5.325

Bhattacharya, S., Alan, P. B., and Paul, M. G. (2003). Cost-effective integration of geologic and petrophysical characterization with material balance and decline curve analysis to develop a 3D reservoir model for PC-based reservoir simulation to design a waterflood in a mature Mississippian carbonate field with limited log data. Paper presented at the AAPG Annual Convention and Exhibit, Salt Lake City, UT.

Bradley, J. S. (1975). Abnormal formation pressure. *AAPG Bulletin*, *59*(6), 957–973.

Buchanan, R. C. (2015). Increased seismicity in Kansas. *The Leading Edge*, *34*(6), 614–617. https://doi.org/10.1190/tle34060614.1

Buckley, C. A., Simpson, A. E., Kerr, C. A., & Schutte, C. F. (1987). The treatment and disposal of waste brine solutions. *Desalination*, *67*, 431–438. https://doi.org/10.1016/0011-9164(87)90260-8

Byerlee, J. (1978). Friction of rocks. *Pure and Applied Geophysics*, *116*(4-5), 615–626. https://doi.org/10.1007/BF00876528

Calais, E., Han, J. Y., DeMets, C., & Nocquet, J. M. (2006). Deformation of the North American plate interior from a decade of continuous GPS measurements. *Journal of Geophysical Research*, *111*, B06402. https://doi.org/10.1029/2005JB004253

Cappa, F., & Rutqvist, J. (2011). Impact of CO_2 geological sequestration on the nucleation of earthquakes. *Geophysical Research Letters*, *38*, L17313. https://doi.org/10.1029/2011GL048487

Carr, T. R., Merriam, D. F., & Bartley, J. D. (2005). Use of relational databases to evaluate regional petroleum accumulation, groundwater flow, and CO_2 sequestration in Kansas. *AAPG Bulletin*, *89*(12), 1607–1627. https://doi.org/10.1306/07190504086

Chiaramonte, L., White, J. A., & Trainor-Guitton, W. (2015). Probabilistic geomechanical analysis of compartmentalization at the Snøhvit CO_2 sequestration project. *Journal of Geophysical Research: Solid Earth*, *120*, 1195–1209. https://doi.org/10.1002/2014JB011376

Cole, V. B. (1975). *Subsurface Ordovician-Cambrian rocks in Kansas*, *Subsurface Geology Series*, (Reprinted 1981 ed., Vol. 2). Lawrence, KS: Kansas Geol. Surv.

Dart, R. L. (1990). In situ stress analysis of wellbore breakouts from Oklahoma and the Texas Panhandle. U.S. Geol. Surv. Bull. 1866, pp. 28.1866-F.

DuBois, S. M., & Wilson, F. W. (1978). List of earthquakes intensities for Kansas, 1867–1977. *Environmental Geological Series 2*. (56 pp.). Kansas Geological Survey.

Ellsworth, W. L. (1982). A general theory for determining the state of stress in the Earth from fault slip measurements. *Terra Cognita*, *2*(2), 170.

Ellsworth, W. L. (2013). Injection-induced earthquakes. *Science*, *341*(6142), 1225942. https://doi.org/10.1126/science.1225942

Ellsworth, W. L., & Zhonghuai, X. (1980). Determination of the stress tensor from focal mechanism data. *Eos, Transactions of the American Geophysical Union*, *61*(1), 117.

Evans, D. M. (1966). The Denver area earthquakes and the Rocky Mountain Arsenal disposal well. *Mountain Geologist*, *3*(1), 23–36.

FazelAlavi, M. (2015). Step-rate test, interference test results and DST results in Wellington, Kansas Geological Survey Open File Report, OF2015-19. Lawrence, KS: University of Kansas.

Franseen, E. K. (2000). A review of Arbuckle Group strata in Kansas from a sedimentologic perspective: Insights for future research from past and recent studies: The compass. *Journal of Earth Sciences Sigma Gamma Epsilon*, *75*(2 & 3), 68–89.

Franseen, E. K., Byrnes, A. P., Cansler, J. R., Steinhauff, D. M., & Carr, T. (2004). The Geology of Kansas–Arbuckle Group. In *Current Research in Earth Sciences: Kansas Geological Survey, Bulletin 250, part 2*. Retrieved from http://www.kgs.ku.edu/Current/2004/franseen/index.html, (last accessed 11/16/2017).

Frohlich, C. (2012). Two-year survey comparing earthquake activity and injection-well locations in the Barnett Shale, Texas. *Proceedings of the National Academy of Sciences of the United States of America*, *109*(35), 13,934–13,938. https://doi.org/10.1073/pnas.1207728109

Gephart, J. W., & Forsyth, D. W. (1984). An improved method for determining the regional stress tensor using earthquake focal mechanism data: Application to the San Fernando earthquake sequence. *Journal of Geophysical Research*, *89*(B11), 9305–9320. https://doi.org/10.1029/JB089iB11p09305

Gerhard, L. C. (2004). *A new look at an old petroleum province*. Lawrence, KS: Kansas Geol. Surv.
Goebel, E. D. (1966). Stratigraphy of Mississippian rocks in western Kansas, (Doctoral dissertation, PhD thesis). Lawrence, KS: University of Kansas.
Goebel, E. D. (1968). Mississippian rocks of western Kansas. *AAPG Bulletin*, *52*(9), 1732–1778.
Grinestaff, G. H., & Caffrey, D. J. (2000). Waterflood management: A case study of the northwest fault block area of Prudhoe Bay, Alaska, using streamline simulation and traditional waterflood analysis. Paper SPE 63152 presented at the SPE Annual Technical Conference and Exhibition, Dallas, TX, 1–4 October. https://doi.org/10.2118/63152-MS
Hanks, T. C., & Bakun, W. H. (2008). M-logA observations for recent large earthquakes. *Bulletin of the Seismological Society of America*, *98*(1), 490–494. https://doi.org/10.1785/0120070174
Healy, J. H., Rubey, W. W., Griggs, D. T., & Raleigh, C. B. (1968). The Denver earthquakes. *Science*, *161*(3848), 1301–1310. https://doi.org/10.1126/science.161.3848.1301
Hildebrand, G. M., Steeples, D. W., Knapp, R. W., Miller, R. D., & Bennett, B. C. (1988). Microearthquakes in Kansas and Nebraska 1977–87. *Seismological Research Letters*, *59*(4), 159–163.
Hinze, W. J. (1963). Regional gravity and magnetic anomaly maps of the Southern Peninsula of Michigan. *Michigan Geological Survey, Report of Investigations* (Vol. 1, pp. 26).
Hinze, W. J., Wold, R. J., & O'Hara, N. W. (1982). Gravity and magnetic anomaly studies of Lake superior. In R. J. Wold & W. J. Hinze (Eds.), *Geology and tectonics of the Lake Superior Basin*, *Geological Society of America Memoir* (Vol. 156, pp. 203–222). Boulder, CO: GSA. https://doi.org/10.1130/MEM156-p203
Holland, A. A. (2013). Optimal fault orientations within Oklahoma. *Seismological Research Letters*, *84*(5), 876–890. https://doi.org/10.1785/0220120153
Holubnyak, Y., Watney, W., Birdie, T., Rush, J., & Fazelalavi, M. (2016). Reservoir modeling of CO_2 injection in Arbuckle saline aquifer at Wellington Field, Sumner County, Kansas, Kansas Geological Survey Open File Report, OF2016-29, Lawrence, KS: University of Kansas.
Horner, D. R. (1951). Pressure Build-Up in Wells. Proceedings Third World Petroleum Congress, The Hague, Sec. II. (pp. 503–23).
Horton, S. (2012). Disposal of hydrofracking waste fluid by injection into subsurface aquifers triggers earthquake swarm in central Arkansas with potential for damaging earthquake. *Seismological Research Letters*, *83*(2), 250–260. https://doi.org/10.1785/gssrl.83.2.250
Keranen, K. M., Savage, H. M., Abers, G. A., & Cochran, E. S. (2013). Potentially induced earthquakes in Oklahoma, USA: Links between wastewater injection and the 2011 M_w 5.7 earthquake sequence. *Geology*, *41*(6), 699–702. https://doi.org/10.1130/G34045.1
Keranen, K. M., Weingarten, M., Abers, G. A., Bekins, B. A., & Ge, S. (2014). Sharp increase in central Oklahoma seismicity since 2008 induced by massive wastewater injection. *Science*, *345*(6195), 448–451. https://doi.org/10.1126/science.1255802
KGS oil and gas wells database (2016). Kansas geological survey. Retrieved from http://www.kgs.ku.edu/Magellan/Qualified/, (accessed 4/1/2016)
Kim, W. Y. (2013). Induced seismicity associated with fluid injection into a deep well in Youngstown, Ohio. *Journal of Geophysical Research: Solid Earth*, *118*, 3506–3518. https://doi.org/10.1002/jgrb.50247
King, E. R., & Zietz, I. (1971). Aeromagnetic study of the midcontinent gravity high of central United States. *Geological Society of America Bulletin*, *82*(8), 2187–2208. https://doi.org/10.1130/0016-7606(1971)82%5B2187:ASOTMG%5D2.0.CO;2
Koester, E. A. (1935). Geology of central Kansas uplift. *AAPG Bulletin*, *19*(10), 1405–1426.
Kruger, J. M. (1997). On-line gravity and magnetic maps of Kansas. *Kansas Geological Survey Open File Report, OF96-51*. Lawrence, KS. University of Kansas.
Lee, W. (1940). The subsurface Mississippian rocks of Kansas. *Kansas Geological Survey Bulletin* (Vol. 33, 114 p.).
Lee, W., & Merriam, D. F. (1954). Preliminary study of the structure of western Kansas: Kansas geological survey. *Oil and Gas Investments*, *11*, 1–23.
Lugn, A. L. (1935). The Pleistocene geology of Nebraska. *Nebraska Geological Survey Bulletin*, *10*, 223.
Lyons, P. L. (1959). The Greenleaf anomaly, a significant gravity feature. In W. W. Hambleton (Ed.), *Symposium on geophysics in Kansas*, *State Geological Survey of Kansas Bulletin* (Vol. 137, pp. 105–120). Lawrence, KS: University of Kansas.
McBee Jr, W. (2003). Nemaha strike-slip fault zone. Paper presented at the AAPG Mid-Continent Section Meeting, Tulsa, OK.
McGarr, A. (1976). Seismic moments and volume changes. *Journal of Geophysical Research*, *81*(8), 1487–1494. https://doi.org/10.1029/JB081i008p01487
McGarr, A. (2014). Maximum magnitude earthquakes induced by fluid injection. *Journal of Geophysical Research: Solid Earth*, *119*, 1008–1019. https://doi.org/10.1002/2013JB010597
McKenzie, D. P. (1969). The relation between fault plane solutions for earthquakes and the directions of the principal stresses. *Bulletin of the Seismological Society of America*, *59*(2), 591–601.
McNamara, D. E., Hayes, G. P., Benz, H. M., Williams, R. A., McMahon, N. D., Aster, R. C., … Earle, P. (2015). Reactivated faulting near Cushing, Oklahoma: Increased potential for a triggered earthquake in an area of United States strategic infrastructure. *Geophysical Research Letters*, *42*, 8328–8332. https://doi.org/10.1002/2015GL064669
Melrose, J. C., & Brandner, C. F. (1974). Role of capillary forces in determining microscopic displacement efficiency for oil recovery by waterflooding. *Journal of Canadian Petroleum Technology*, *13*(4), 54–62.
Merriam, D. F. (1956). History of earthquakes in Kansas. *Bulletin of the Seismological Society of America*, *46*(2), 87–96.
Merriam, D. F. (1963). *The geologic history of Kansas*, *State Geological Survey of Kansas Bulletin*, (Vol. 162, p. 317). Lawrence, KS: University of Kansas.
Michael, A. J. (1984). Determination of stress from slip data: Faults and folds. *Journal of Geophysical Research*, *89*(B13), 11517–11526. https://doi.org/10.1029/JB089iB13p11517
Michael, A. J. (1987). Use of focal mechanisms to determine stress: A control study. *Journal of Geophysical Research*, *92*(B1), 357–368. https://doi.org/10.1029/JB092iB01p00357
Midwest Governors Association and Great Plains Institute (2012). CO_2-EOR potential in the MGA region. Retrieved from http://www.midwesterngovernors.org/Publications/EOR2011.pdf (Accessed 07/24/2017)
Moos, D., & Zoback, M. D. (1990). Utilization of observations of well bore failure to constrain the orientation and magnitude of crustal stresses: Application to continental, Deep Sea Drilling Project, and Ocean Drilling Program boreholes. *Journal of Geophysical Research*, *95*(B6), 9305–9325. https://doi.org/10.1029/JB095iB06p09305
Morris, A., Ferrill, D. A., & Henderson, D. B. (1996). Slip-tendency analysis and fault reactivation. *Geology*, *24*(3), 275–278. https://doi.org/10.1130/0091-7613(1996)024%3C0275:STAAFR%3E2.3.CO;2
Morris, J. P., Hao, Y., Foxall, W., & McNab, W. (2011). A study of injection-induced mechanical deformation at the In Salah CO_2 storage project. *International Journal of Greenhouse Gas Control*, *5*(2), 270–280. https://doi.org/10.1016/j.ijggc.2010.10.004

Morris, W., Leung, B., Furukawa, H., Yaghi, O. K., He, N., Hayashi, H., … Yaghi, O. M. (2010). A combined experimental-computational investigation of carbon dioxide capture in a series of isoreticular zeolitic imidazolate frameworks. *Journal of the American Chemical Society*, *132*(32), 11,006–11,008. https://doi.org/10.1021/ja104035j

Morrow, N. R. (1990). Wettability and its effect on oil recovery. *Journal of Petroleum Technology*, *42*(12), 1–476.

Nasralla, R. A., Snippe, J. R., and Farajzadeh, R. (2015). Coupled geochemical-reservoir model to understand the interaction between low salinity brines and carbonate rock. Paper presented at SPE Enhanced Oil Recovery Conference, Kuala Lumpur, Malaysia.

Nelson, E. J., Chipperfield, S. T., Hillis, R. R., Gilbert, J., McGowen, J., & Mildren, S. D. (2007). The relationship between closure pressures from fluid injection tests and the minimum principal stress in strong rocks. *International Journal of Rock Mechanics and Mining Sciences*, *44*(5), 787–801. https://doi.org/10.1016/j.ijrmms.2006.10.004

Nelson, P. H., & Gianoutsos, N. J. (2011). Evolution of overpressured and underpressured oil and gas reservoirs, Anadarko Basin of Oklahoma, Texas, and Kansas. United States Geological Survey Open File Report 2011-1245, 3 sheets.

Oray, E., Hinze, W. J., & O'Hara, N. O. (1973). Gravity and magnetic evidence for the eastern termination of the Lake Superior syncline. *Geological Society of America Bulletin*, *84*(8), 2763–2780. https://doi.org/10.1130/0016-7606(1973)84%3C2763:GAMEFT%3E2.0.CO;2

Puckette, J., and Al-Shaieb, Z. (2003). Naturally underpressured reservoirs: Applying the compartment concept to the safe disposal of liquid waste. Paper presented at the Southwest Section Meeting of the AAPG, Fort Worth, TX.

Raleigh, C. B., Healy, J. H., & Bredehoeft, J. D. (1976). An experiment in earthquake control at Rangely, Colorado. *Science*, *191*(4233), 1230–1237. https://doi.org/10.1126/science.191.4233.1230

Reasenberg, P. A., & Simpson, R. W. (1992). Response of regional seismicity to the static stress change produced by the Loma Prieta earthquake. *Science*, *255*(5052), 1687–1690. https://doi.org/10.1126/science.255.5052.1687

Rubinstein, J. L., Ellsworth, W. L., McGarr, A., & Benz, H. M. (2014). The 2001–present induced earthquake sequence in the Raton Basin of northern New Mexico and southern Colorado. *Bulletin of the Seismological Society of America*, *104*(5), 2162–2181. https://doi.org/10.1785/0120140009

Scheffer, A. (2012). Geochemical and microbiological characterization of the Arbuckle saline aquifer, a potential CO_2 storage reservoir; implications for hydraulic separation and caprock integrity, (Master thesis). Lawrence, KS: Department of Geology, University of Kansas.

Seeber, L., & Armbruster, J. G. (2000). Earthquakes as beacons of stress change. *Nature*, *407*(6800), 69–72. https://doi.org/10.1038/35024055

Shipton, Z. K., Evans, J. P., Dockrill, B., Heath, J., Williams, A., Kirchner, D., & Kolesar, P. T. (2006). Natural leaking CO_2-charged systems as analogs for failed geologic storage reservoirs. In D. C. Thomas & S. M. Benson (Eds.), *Carbon dioxide capture for storage in deep geologic formations–Results from the CO_2 capture project* (Vol. 2, pp. 699–712). Oxford, UK: Elsevier.

Smithson, S. B. (1971). Densities of metamorphic rocks. *Geophysics*, *36*(4), 690–694. https://doi.org/10.1190/1.1440205

Sorenson, R. P. (2005). A dynamic model for the Permian Panhandle and Hugoton fields, western Anadarko basin. *AAPG Bulletin*, *89*(7), 921–938. https://doi.org/10.1306/03010504045

Stander, T. W., & Grant, J. L. (1989). A case history of petroleum exploration in the southern Forest City basin using gravity and magnetic surveys. In D. W. Steeples (Ed.), *Geophysics in Kansas*, *Kansas Geological Survey Bulletin* (Vol. 226, pp. 245–256). Lawrence, KS: University of Kansas.

Steeples, D. W., & Brosius, L. (1996). *Earthquakes*, *Kansas Geological Survey, Public Information Circular 3*, (6 p.).

Steeples, D. W., DuBois, S. M., & Wilson, F. W. (1979). Seismicity, faulting, and geophysical anomalies in Nemaha County, Kansas: Relationship to regional structures. *Geology*, *7*(3), 134–138. https://doi.org/10.1130/0091-7613(1979)7%3C134:SFAGAI%3E2.0.CO;2

Stein, R. S. (1999). The role of stress transfer in earthquake occurrence. *Nature*, *402*(6762), 605–609. https://doi.org/10.1038/45144

Stein, S., & Wysession, M. (2009). *An introduction to seismology, earthquakes, and earth structure*. Malden, MA: John Wiley.

Streit, J. E., & Hillis, R. R. (2004). Estimating fault stability and sustainable fluid pressures for underground storage of CO_2 in porous rock. *Energy*, *29*(9-10), 1445–1456. https://doi.org/10.1016/j.energy.2004.03.078

Tang, G. Q., & Morrow, N. R. (1997). Salinity, temperature, oil composition, and oil recovery by waterflooding. *SPE Reservoir Engineering*, *12*(04), 269–276. https://doi.org/10.2118/36680-PA

Thiel, E. (1956). Correlation of gravity anomalies with the Keweenawan geology of Wisconsin and Minnesota. *Geological Society of America Bulletin*, *67*(8), 1079–1100. https://doi.org/10.1130/0016-7606(1956)67%5B1079:COGAWT%5D2.0.CO;2

Tingay, M., Reinecker, J., and Müller, B. (2008). Borehole breakout and drilling-induced fracture analysis from image logs. World Stress Map Project, 1-8.

Townend, J., & Zoback, M. D. (2000). How faulting keeps the crust strong. *Geology*, *28*(5), 399–402. https://doi.org/10.1130/0091-7613(2000)28%3C399:HFKTCS%3E2.0.CO;2

Vavryčuk, V. (2014). Iterative joint inversion for stress and fault orientations from focal mechanisms. *Geophysical Journal International*, *199*(1), 69–77. https://doi.org/10.1093/gji/ggu224

Vilarrasa, V., Olivella, S., Carrera, J., & Rutqvist, J. (2014). Long term impacts of cold CO_2 injection on the caprock integrity. *International Journal of Greenhouse Gas Control*, *24*, 1–13. https://doi.org/10.1016/j.ijggc.2014.02.016

Walters, R. F. (1958). Differential entrapment of oil and gas in Arbuckle dolomite of central Kansas. *AAPG Bulletin*, *42*(9), 2133–2173.

Weingarten, M., Ge, S., Godt, J. W., Bekins, B. A., & Rubinstein, J. L. (2015). High-rate injection is associated with the increase in US mid-continent seismicity. *Science*, *348*(6241), 1336–1340. https://doi.org/10.1126/science.aab1345

Wells, D. L., & Coppersmith, K. J. (1994). New empirical relationships among magnitude, rupture length, rupture width, rupture area, and surface displacement. *Bulletin of the Seismological Society of America*, *84*(4), 974–1002.

Wiprut, D., & Zoback, M. (2000). Constraining the stress tensor in the Visund field, Norwegian North Sea: Application to wellbore stability and sand production. *International Journal of Rock Mechanics and Mining Sciences*, *37*(1-2), 317–336. https://doi.org/10.1016/S1365-1609(99)00109-4

Woelk, T. S., & Hinze, W. J. (1995). Midcontinent rift system in northeastern Kansas. In N. L. Anderson & D. E. Hedke (Eds.), *Geophysical atlas of selected oil and gas fields in Kansas*, *Kansas Geological Survey Bulletin* (Vol. 22, pp. 22–27). Lawrence, KS: Kansas Geological Survey and Kansas Geological Society.

Worum, G., van Wees, J. D., Bada, G., van Balen, R. T., Cloetingh, S., & Pagnier, H. (2004). Slip tendency analysis as a tool to constrain fault reactivation: A numerical approach applied to three-dimensional fault models in the Roer Valley rift system (southeast Netherlands). *Journal of Geophysical Research*, *109*, B02401. https://doi.org/10.1029/2003JB002586

Yeck, W. L., Weingarten, M., Benz, H. M., Mcnamara, D. E., Bergman, E., Herrmann, R. B., … Earle, P. S. (2016). Far-field pressurization likely caused one of the largest injection induced earthquakes by reactivating a large pre-existing basement fault structure. *Geophysical Research Letters*, *43*, 10,198–10,207. https://doi.org/10.1002/2016GL070861

Yeck, W. L., Hayes, G. P., McNamara, D. E., Rubinstein, J. L., Barnhart, W. D., Earle, P. S., & Benz, H. M. (2017). Oklahoma experiences largest earthquake during ongoing regional wastewater injection hazard mitigation efforts. *Geophysical Research Letters*, *44*, 711–717. https://doi.org/10.1002/2016GL071685

Yih-Hsiung, Y., Eric, B., Lin, C. H., & Jacques, A. (1991). Stress tensor analysis in the Taiwan area from focal mechanisms of earthquakes. *Tectonophysics*, *200*(1-3), 267–280. https://doi.org/10.1016/0040-1951(91)90019-O

Zeller, D. E. (1968). The stratigraphic succession in Kansas. *Kansas Geological Survey Bulletin*, *189*. 81

Zhang, Y., Person, M., Rupp, J., Ellett, K., Celia, M. A., Gable, C. W., … Dewers, T. (2013). Hydrogeologic controls on induced seismicity in crystalline basement rocks due to fluid injection into basal reservoirs. *Groundwater*, *51*(4), 525–538. https://doi.org/10.1111/gwat.12071

Zoback, M. L. (1992). First-and second-order patterns of stress in the lithosphere: The World Stress Map Project. *Journal of Geophysical Research*, *97*(B8), 11,703–11,728. https://doi.org/10.1029/92JB00132

Zoback, M. D., Barton, C. A., Brudy, M., Castillo, D. A., Finkbeiner, T., Grollimund, B. R., & Wiprut, D. J. (2003). Determination of stress orientation and magnitude in deep wells. *International Journal of Rock Mechanics and Mining Sciences*, *40*(7-8), 1049–1076. https://doi.org/10.1016/j.ijrmms.2003.07.001

Zoback, M. D., & Gorelick, S. M. (2012). Earthquake triggering and large-scale geologic storage of carbon dioxide. *Proceedings of the National Academy of Sciences*, *109*(26), 10,164–10,168. https://doi.org/10.1073/pnas.1202473109

Zoback, M. D., Moos, D., Mastin, L., & Anderson, R. N. (1985). Well bore breakouts and in situ stress. *Journal of Geophysical Research*, *90*(B7), 5523–5530. https://doi.org/10.1029/JB090iB07p05523

Zoback, M. D., Townend, J., & Grollimund, B. (2002). Steady-state failure equilibrium and deformation of intraplate lithosphere. *International Geology Review*, *44*(5), 383–401. https://doi.org/10.2747/0020-6814.44.5.383

Zoback, M. L., & Zoback, M. (1980). State of stress in the conterminous United States. *Journal of Geophysical Research*, *85*(B11), 6113–6156. https://doi.org/10.1029/JB085iB11p06113

Zoback, M. D., & Zoback, M. L. (1991). Tectonic stress field of North America and relative plate motions. In D. B. Slemmons, et al. (Eds.), *Neotectonics of North America* (pp. 339–366). Boulder, CO: Geological Society of America.

Zoback, M. L., Zoback, M. D., Adams, J., Assumpcao, M., Bell, S., Bergman, E. A., & Fuchs, K. (1989). Global patterns of tectonic stress. *Nature*, *341*(6240), 291–298. https://doi.org/10.1038/341291a0

Zoback, M., Zoback, M., Eaton, J., Mount, V., & Suppe, J. (1987). New evidence on the state of stress of the San Andreas Fault system. *Science*, *238*(4830), 1105–1111. https://doi.org/10.1126/science.238.4830.1105